UNIVERSITY OF ALBERTA
LIBRARY

Regulations Regarding Theses and Dissertations

Typescript copies of theses and dissertations for Master's and Doctor's degrees deposited in the University of Alberta Library, as the official Copy of the Faculty of Graduate Studies, may be consulted in the Reference Reading Room only.

A second copy is on deposit in the Department under whose supervision the work was done. Some Departments are willing to loan their copy to libraries, through the inter-library loan service of the University of Alberta Library.

These theses and dissertations are to be used only with due regard to the rights of the author. Written permission of the author and of the Department must be obtained through the University of Alberta Library when extended passages are copied. When permission has been granted, acknowledgement must appear in the published work.

This thesis or dissertation has been used in accordance with the above regulations by the persons listed below. The borrowing library is obligated to secure the signature of each user.

Please sign below:

Date	Signature	Institution

THE UNIVERSITY OF ALBERTA

CONVERTED-WAVE METHOD FOR DETERMINING CRUSTAL STRUCTURE IN SOUTHERN ALBERTA

by

N. NAVEENA CHANDRA

A THESIS
SUBMITTED TO THE FACULTY OF GRADUATE STUDIES
IN PARTIAL FULFILLMENT OF THE REQUIREMENTS FOR THE DEGREE
OF MASTER OF SCIENCE

DEPARTMENT OF PHYSICS
EDMONTON, ALBERTA
SEPTEMBER, 1966

UNIVERSITY OF ALBERTA

FACULTY OF GRADUATE STUDIES

The undersigned certify that they have read, and recommend to the Faculty of Graduate Studies for acceptance, a thesis entitled CONVERTED-WAVE METHOD FOR DETERMINING CRUSTAL STRUCTURE IN SOUTHERN ALBERTA, submitted by N. Naveena Chandra, in partial fulfillment of the requirements for the degree of Master of Science.

ACKNOWLEDGEMENTS

With sincere and deep appreciation I wish to thank Dr. G.L. Cumming whose guidance, work and encouragement have been invaluable throughout the entire programme.

Messrs. Stanley Allen and Charles McCloughan, the recording truck operators, of the field season 1965, and Messrs. D. Robertson and G.T.F.R. Maureau of the field season 1963, are to be thanked for the seismic records they made. In addition, Mr. Robertson did an excellent job with drafting of several of the diagrams used in this work.

A special vote of thanks is to be extended to the many other persons who assisted in the field operation.

Records obtained by the personnel from the United States Geological Survey have been used as part of the investigations. They must be commended for the quality of the records.

Century Geophysical Corporation of Canada furnished the drilling rigs and technical personnel necessary for the emplacement and detonation of the explosives.

During the course of his research, the author was supported by a Graduate Teaching Assistantship from the Department of Physics, University of Alberta.

I am deeply indebted to Mrs. L. Medford for the admirable job she has done in typing the thesis.

The present work is part of a project sponsored by the National Research Council of Canada, the Defence Research Board of Canada; and the Advanced Research Projects Agency, Project Vela-Uniform.

CONTENTS

LIST OF ILLUSTRATIONS

CHAPTER I

INTRODUCTION

If one accepts the uniformitarian theory of the evolution of the earth, then earthquakes have occurred throughout the long history of the earth, as they do at the present time. The recorded evidence for the occurrence of earthquakes only dates back to a few millennia. Branson et al. (1955), make the mention of earthquake occurrences as reported by historians such as Pliny and Herodotus dating back 2500 years. That earthquakes release energy and give rise to elastic waves has been known only for the last few centuries and detailed studies of the propagation of these elastic waves have only been carried out relatively recently, having been begun by such workers as Rayleigh, Love, Lamb, and Jeffreys. Seismic waves generated by earthquakes have been used extensively to study the details of the crust of the earth. Mohorovičić was one of the first to demonstrate the existence of a crust of lower velocity material overlying a higher velocity mantle.

One of the major difficulties in utilizing earthquake waves to study crustal structure is the uncertainty in both time and location of the energy release. Thus in recent years investigators have come to rely more and more on man-made explosions where both the location and time of the explosion are accurately known.

Geologists have shown that the sedimentary rocks near the surface of the earth are often layered with a particular rock unit a few tens of feet thick often occurring over an area of many tens or even hundreds of square miles. Thus the concept of plane horizontal layers is a justifiable one near the surface of the earth. Travel-time curves for the acoustic waves from earthquakes and man-made explosions often suggest that the earth is layered even below this upper sedimentary section and thus the assumption of layering of the crust as a whole is a common, and useful approximation.

In an elastic solid, two types of waves may be propagated, longitudinal or P-wave, and shear or S-wave. There is a considerable body of work (an extensive list of references is given by Ewing et al., 1957), both theoretical and experimental, dealing with the reflection and refraction of these elastic waves at the boundaries of various layers. Waves incident on an interface with the source of disturbance, say in the first medium, are refracted and reflected at the interface depending on the boundary conditions. In the case of acoustic waves one often makes use of the critical angle as used in optics. When the angle of the incident wave is equal to the critical angle, the elastic waves travel along the boundary, and are then returned into the medium in which the source is located, as so-called head waves. These waves can undergo conversion at the interface from P to S or vice versa depending again on boundary conditions. The present investigations deal with these converted phases.

The crustal structure of Southern Alberta, based on the refraction waves generated by explosions, has been the subject of several investigations (Weaver 1962, and Maureau 1964), and these results have been reported in papers by members of the Physics Department, University of Alberta (1962, 1964, 1966). Fig. I. 1 shows the location of various profiles shot in the general area of Southern Alberta and Saskatchewan. Bow City Shot Point and Suffield Shot Point locations can be seen in this map.

The present work is based on data from two refraction profiles in Southern Alberta. One profile utilizes recordings of seismic waves produced by a 500 ton charge of TNT exploded on the surface at the Suffield experimental station of the Defence Research Board, and recorded in the foothills and Rocky Mountains; the other consists of recordings from a series of buried charges of various sizes up to 1000 pounds, at a shot point near the town of Bow City. The detector locations for the second profile are in approximately the same place as those for the first and thus direct comparison can be made between the data on each profile. Unfortunately the profiles are shot in the same direction and this results in an uncertainty in the dip of the various layers from which arrivals have been detected. However the records examined furnish excellent opportunities for the study of later events which throw considerable light on the structure. In principle it should be possible to resolve the uncertainties of dip by utilizing converted phases, but in practice this appears to be difficult.

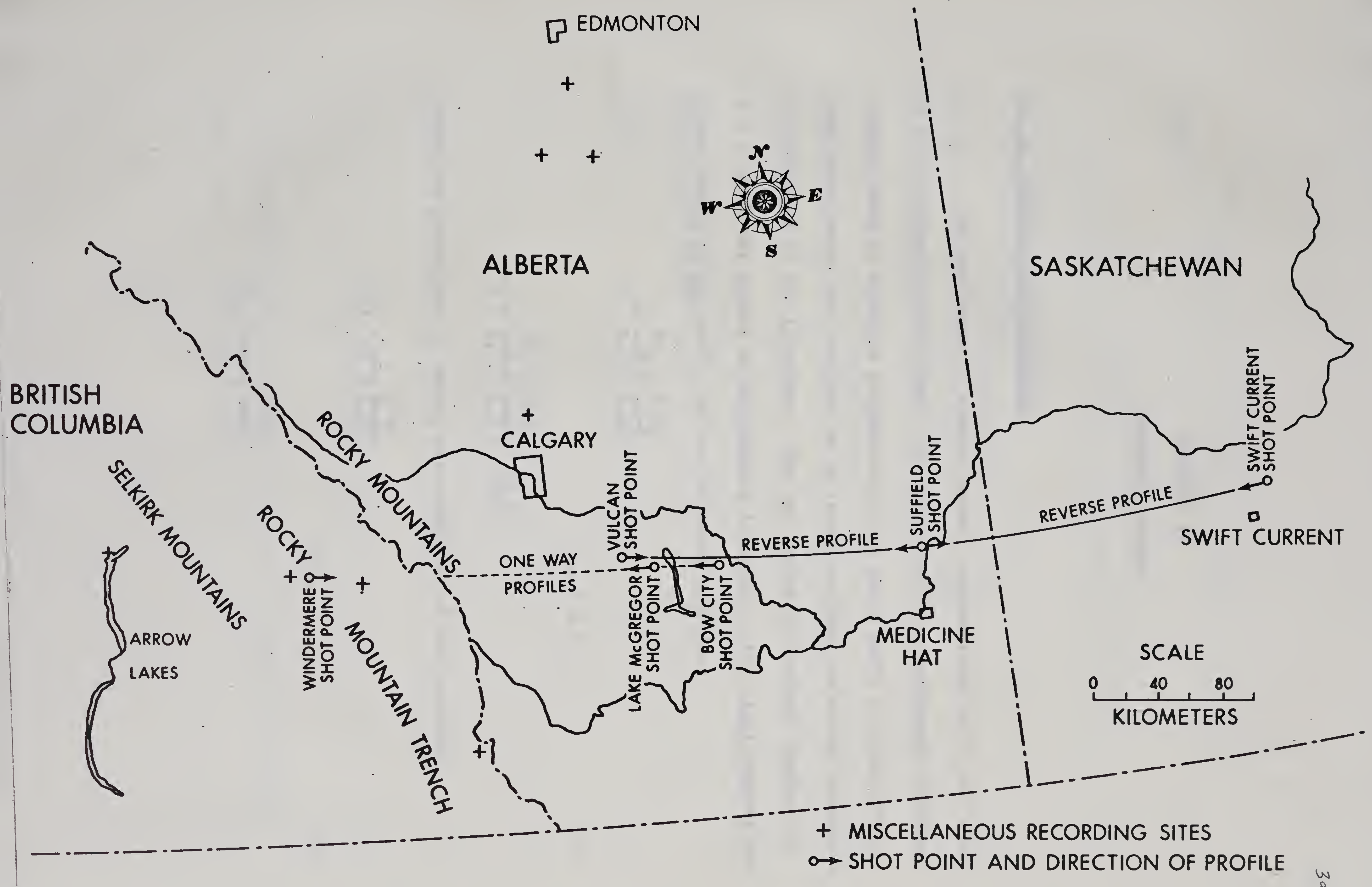

LOCATION MAP

CHAPTER II

CONVERTED PHASES

II. 1 General Considerations

II. 1. 1 The two types of elastic waves, compressional or P, and shear or S, are known as body waves. An explosion or an earthquake releases energy, some of which is propagated in the rigid earth by these waves. When these waves are incident on an interface they are either refracted, or reflected at the interface. For two layers in "welded" contact at z = 0, with the source of disturbance in layer 1, the displacements are given (Ewing et al. 1957), by the following equations.

$$q_i = \frac{\partial \phi_i}{\partial r} + \frac{\partial^2 \psi_i}{\partial r \partial z}$$

$$\text{for } i = 1, 2 \qquad (1)$$

$$w_i = \frac{\partial \phi_i}{\partial z} + \frac{\partial^2 \psi_i}{\partial z^2} + k_{\beta_i}^2 \psi_i$$

where the potentials ϕ_i and ψ_i are solutions of the equations

$$\nabla^2 \phi_i = \frac{1}{\alpha_i^2} \frac{\partial^2 \phi_i}{\partial t^2}$$

$$\text{for } i = 1, 2 \qquad (2)$$

$$\nabla^2 \psi_i = \frac{1}{\beta_i^2} \frac{\partial^2 \psi_i}{\partial t^2}$$

Ewing <u>et al.</u> give the following solutions for the above equations

$$\phi_1 = \int_0^\infty \frac{k}{\nu_1} J_o(kr) e^{-\nu_1 |z-h|} dk + \int_0^\infty Q_1(k) J_o(kr) e^{-\nu_1 (z-h)} dk \tag{3}$$

$$\psi_1 = \int_0^\infty S_1(k) J_o(kr) e^{-\nu_1'(z-h)} dk \tag{4}$$

(3) and (4) hold for $z > 0$

$$\phi_2 = \int_0^\infty Q_2(k) J_o(kr) e^{\nu_2 (z-h)} dk \tag{5}$$

$$\psi_2 = \int_0^\infty S_2(k) J_o(kr) e^{\nu_2'(z-h)} dk \tag{6}$$

(5) and (6) hold for $z < 0$

where

$$\nu_1' = \sqrt{k^2 - k_{\beta_1}^2} \tag{7}$$

$$\nu_2' = \pm \sqrt{k^2 - k_{\beta_2}^2} \tag{8}$$

$$\nu_1 = \sqrt{k^2 - k_{\alpha_1}^2} \tag{9}$$

$$\nu_2 = \sqrt{k^2 - k_{\alpha_2}^2} \tag{10}$$

The four coefficients Q_i, S_i can be chosen to satisfy the boundary conditions.

At $z = 0$,

$$q_1 = q_2 \quad \text{and} \quad w_1 = w_2 \tag{11}$$
$$(P_{zz})_1 = (P_{zz})_2 \quad \text{and} \quad (P_{zr})_1 = (P_{zr})_2$$

(11) merely state that the displacements and stresses are continuous across the interface.

Hence we have

$$\frac{\partial\phi_1}{\partial r} + \frac{\partial^2\psi_1}{\partial z\partial r} = \frac{\partial\phi_2}{\partial r} + \frac{\partial^2\psi_2}{\partial z\partial r} \tag{12}$$

$$\frac{\partial\phi_1}{\partial z} + \frac{\partial^2\psi_1}{\partial z^2} + k_{\beta_1}{}^2\psi_1 = \frac{\partial\phi_2}{\partial z} + \frac{\partial^2\psi_2}{\partial z^2} + k_{\beta_2}{}^2\psi_2 \tag{13}$$

$$\lambda_1\nabla^2\phi_1 + 2\mu_1 \frac{\partial w_1}{\partial z} = \lambda_2\nabla^2\phi_2 + 2\mu_2 \frac{\partial w_2}{\partial z} \tag{14}$$

$$\mu_1 \left(\frac{\partial q_1}{\partial z} + \frac{\partial w_1}{\partial r}\right) = \mu_2 \left(\frac{\partial q_2}{\partial z} + \frac{\partial w_2}{\partial r}\right) \tag{15}$$

Since ϕ_1, ψ_1, ϕ_2 and ψ_2 are given by (3), (4), (5) and (6) above, one can differentiate these functions with respect to z and r, and by using the properties of Bessel's Functions one can show that (12) to (15) are reduced to

$$\hat{Q}_1 - \hat{Q}_2 - \nu_1'\hat{S}_1 - \nu_2'\hat{S}_2 = -\frac{k}{\nu_1} e^{-\nu_1 h} \tag{16}$$

$$\nu_1\hat{Q}_1 + \nu_2\hat{Q}_2 - k^2\hat{S}_1 + k^2\hat{S}_2 = ke^{-\nu_1 h} \tag{17}$$

$$-(2\mu_1k^2-\rho_1w^2)\hat{Q}_1+(2\mu_2k^2-\rho_2w^2)\hat{Q}_2+2\mu_1k^2\nu_1'S_1$$

$$+2\mu_2k^2\nu_2'\hat{S}_2=\frac{k}{\nu_1}(2\mu_1k^2-\rho_1w^2)e^{-\nu_1h} \tag{18}$$

$$2\mu_1\nu_1\hat{Q}_1+2\mu_2\nu_2\hat{Q}_2-(2\mu_1k^2-\rho_1w^2)\hat{S}_1+(2\mu_2k^2-\rho_2w^2)\hat{S}_2=2k\mu_1e^{-\nu_1h} \tag{19}$$

where

$$\hat{Q}_1=Q_1e^{\nu_1h}\;;\qquad \hat{Q}_2=Q_2e^{-\nu_2h}$$

$$\hat{S}_1=S_1e^{\nu_1'h}\;;\qquad \hat{S}_2=S_2e^{-\nu_2'h}$$

If we now put (Ewing *et al.*)

$$2\mu_1k^2-\rho_1w^2=a_1\;;\quad 2\mu_2k^2-\rho_2w^2=a_2\,,$$

then the determinant of the above systems of equations (16) to (19) is given by

$$\Delta(k)=\begin{vmatrix} 1 & -1 & -\nu_1' & -\nu_2' \\ \nu_1 & \nu_2 & -k^2 & k^2 \\ -a_1 & a_2 & 2\mu_1k^2\nu_1' & 2\mu_2k^2\nu_2' \\ 2\mu_1\nu_1 & 2\mu_2\nu_2 & -a_1 & a_2 \end{vmatrix}$$

Using Kramer's Rule we can now write down the coefficients Q_i and S_i as follows.

$$Q_1=\frac{\Delta_1}{\Delta}e^{-2\nu_1h}\qquad S_1=\frac{\Delta_1'}{\Delta}e^{-(\nu_1+\nu_1')h}$$

$$Q_2 = \frac{\Delta_2}{\Delta} e^{-(\nu_1-\nu_2)h} \qquad S_2 = \frac{\Delta_2'}{\Delta} e^{-(\nu_1-\nu_2')h}$$

where

$$\Delta_1 = \begin{vmatrix} -1 & -\nu_1' & -\nu_2' & -\dfrac{k}{\nu_1} \\ \nu_2 & -k^2 & k^2 & k \\ a_2 & 2\mu_1 k^2 \nu_1' & 2\mu_2 k^2 \nu_2' & \dfrac{ka_1}{\nu_1} \\ 2\mu_2\nu_2 & -a_1 & a_2 & 2k\mu_1 \end{vmatrix}$$

$$\Delta_2 = \begin{vmatrix} -\nu_1' & -\nu_2' & -k/\nu_1 & 1 \\ -k^2 & k^2 & k & \nu_1 \\ 2\mu_1 k^2 \nu_1' & 2\mu_2 k^2 \nu_2' & \dfrac{ka_1}{\nu_1} & -a_1 \\ -a_1 & a_2 & 2k\mu_1 & 2\mu_1\nu_1 \end{vmatrix}$$

Two similar expressions can be given for Δ_1' and Δ_2'. Therefore we can write down, following Ewing et al., (3), (4), (5) and (6) as

$$\phi_1 = \int_0^\infty \frac{k}{\nu_1} J_0(kr) e^{-\nu_1|z-h|} dk + \int_0^\infty \frac{\Delta_1}{\Delta} J_0(kr) e^{-\nu_1(z+h)} dk \qquad (20)$$

$$\psi_1 = \int_0^\infty \frac{\Delta_1'}{\Delta} J_0(kr) e^{-\nu_1' z-\nu_1 h} dk \qquad (21)$$

$$\phi_2 = \int_0^\infty \frac{\Delta_2}{\Delta} J_0(kr) e^{\nu_2 z-\nu_1 h} dk \qquad (22)$$

$$\psi_2 = \int_o^\infty \frac{\Delta_2'}{\Delta} J_o(kr) e^{\nu_2' z - \nu_1 h} dk \qquad (23)$$

The first term in (20) represents the compressional wave. All other terms in (20) to (23) represent, according to Ewing *et al.*, waves generated by it. To investigate these waves one has to insert the time factor and carry out the integration. Different types of waves are determined by a set of branch line integrals corresponding to $K = K_{\alpha_1}$, K_{β_1}, K_{α_2} and K_{β_2} and by residues corresponding to roots of the equation

$$\Delta\ (k) = 0$$

Or $\Delta(k)$ can be given by

$$\Delta(k) = 0 = 4(\mu_2 - \mu_1)^2 \{[k^2(k^2 - \frac{w^2(\rho_2 - \rho_1)}{2(\mu_2 - \mu_1)})^2 - \nu_1\nu_1'[k^2 - \frac{\rho_2 w^2}{2(\mu_2 - \mu_1)}]^2$$

$$- \nu_2\nu_2'[k^2 + \frac{\rho_1 w^2}{2(\mu_2 - \mu_1)}]^2 - (\nu_1\nu_2' + \nu_2\nu_1')\frac{w^4\rho_1\rho_2}{4(\mu_2 - \mu_1)^2} + \nu_1\nu_2\nu_1'\nu_2' k^2\}$$

K has four roots and accordingly we have four cases, each case corresponding to a wave type.

One can consider the wave path as composed of three parts. One from source to interface, second along the interface and third from interface to detector. The coefficient of h in the exponential states whether the first part is compressional or shear wave. The coefficient of z in the exponential gives the same information about the third part, while the value of 'k' at the branch point indicates the mode of travel along the interface. If we have two media with com-

pressional wave velocities V_1, and V_2 and shear wave velocities v_1, v_2 and such that $V_2 > v_2 > V_1 > v_1$ then there is a possibility of shear wave along the interface as well. In the case of the earth one rarely comes across two media such that the shear wave velocity in the lower medium is greater than the compressional wave velocity in the upper medium, so that if the wave travelling along the boundary of the lower medium is a shear wave it cannot give rise to, or be induced by, a compressional wave in the upper medium. This limits the number of possible cases to the wave types shown in Figure II.1. If the layer boundary is horizontal, 2) and 3) will arrive simultaneously and the only means of distinguishing between them will be an analysis of the particle motion at the detector.

Waves of types 1) to 4) will have the same velocity across the spread of detectors if there is no dip, but those waves having one or more paths in the upper medium as an S wave, will be delayed with respect to the P wave by an amount which depends on Poissons's ratio in the upper layer and on the thickness of the upper layer. The analysis of crustal structure is based on these time differences.

In general there may be several layers above the refracting horizon, so there will exist the possibility of further conversions at each of the interfaces. Boundary conditions will determine the relative amounts of energy in each of these possible waves and hence will determine whether any particular wave type may be detected at the surface.

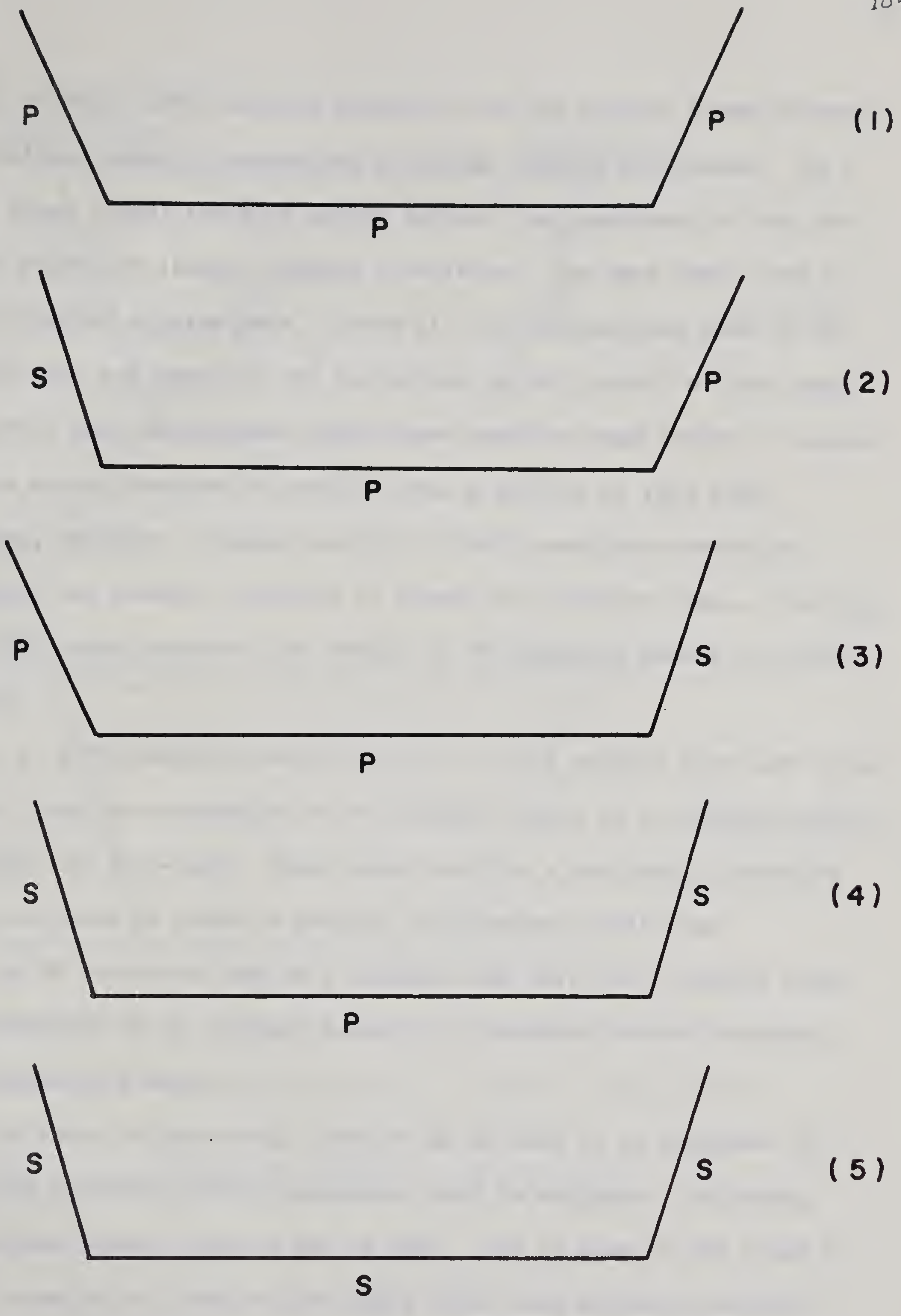

Fig. II. 1

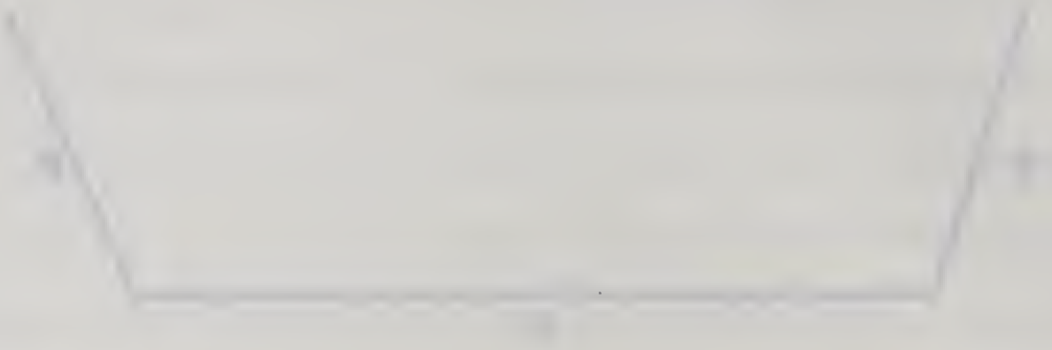

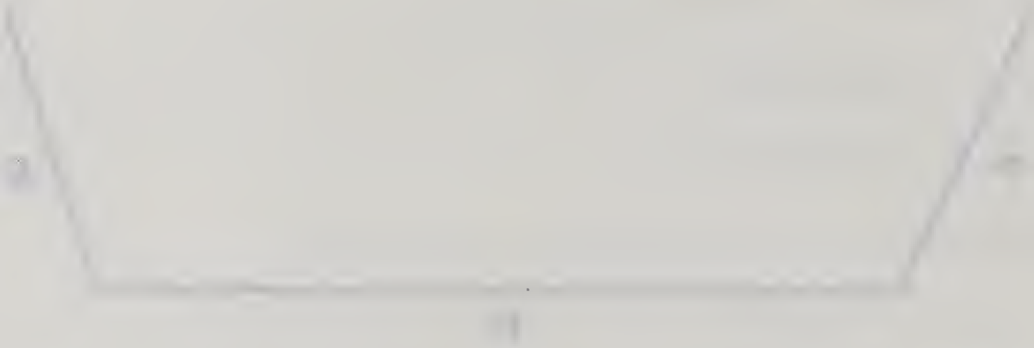

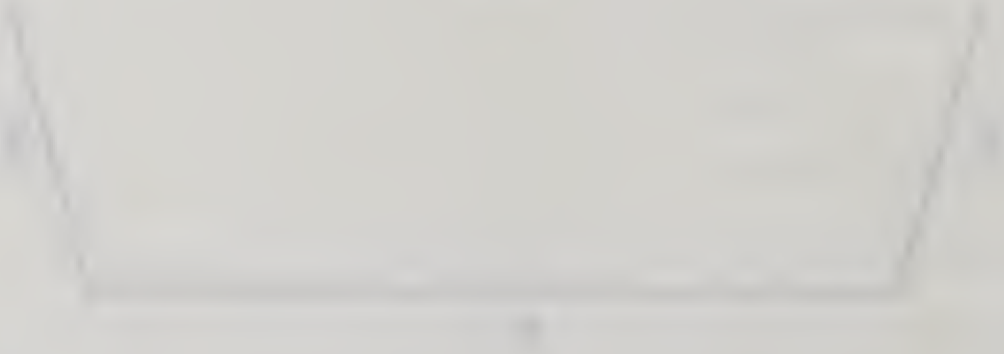

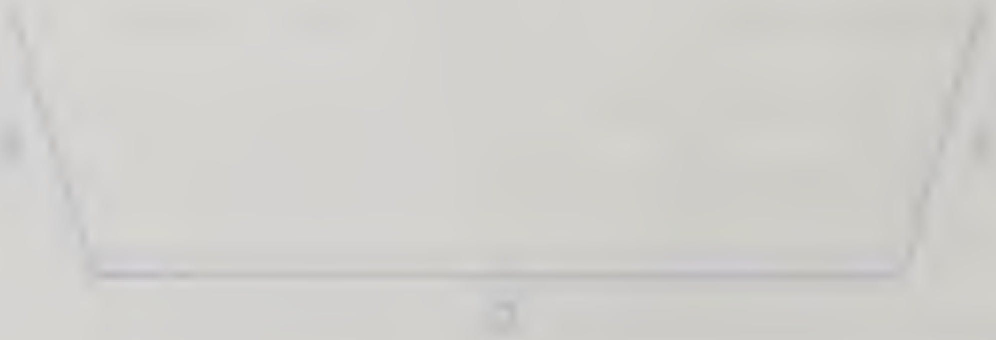

II. 1. 2 Hall (1964) derived equations for the arrival times of waves for various cases of conversions at gently dipping interfaces. In a later paper (1966) the same author derives the equations for the converted phases at steeply dipping interfaces. The case dealt here is that of gently dipping beds. Hence all the calculations made in the present work are based on the derivations given in Hall's first paper (op. cit.) Hall and Brisbin (1965) have used the same theory to explain various events observed on records from a profile at Flin Flon-Mafeking, Manitoba. Pakiser and Hill (1963) used later events to interpret the crustal structure in Nevada and Southern Idaho. Cook *et al.* (1962) have discussed the status of PS converted phases in crustal studies.

II. 1. 3 A PS converted wave (Fig. II. 2) is a seismic body wave which results from the conversion of an incident P-wave at a boundary within the crust, to an S-wave. This S-wave must be a vertically polarized shear or S_V wave in order to satisfy the boundary conditions.

An SP converted wave is a seismic body wave which results from the conversion of an incident S-wave at a boundary within the crust, to a refracted P-wave.

In order to positively identify an S_V wave it is important to note that horizontal motion geophones must be employed. Following this several other criteria may be used. One of them is the study of particle motion to confirm that these waves have motions consistent with S_V waves. The second is the study of the amplitude relationships.

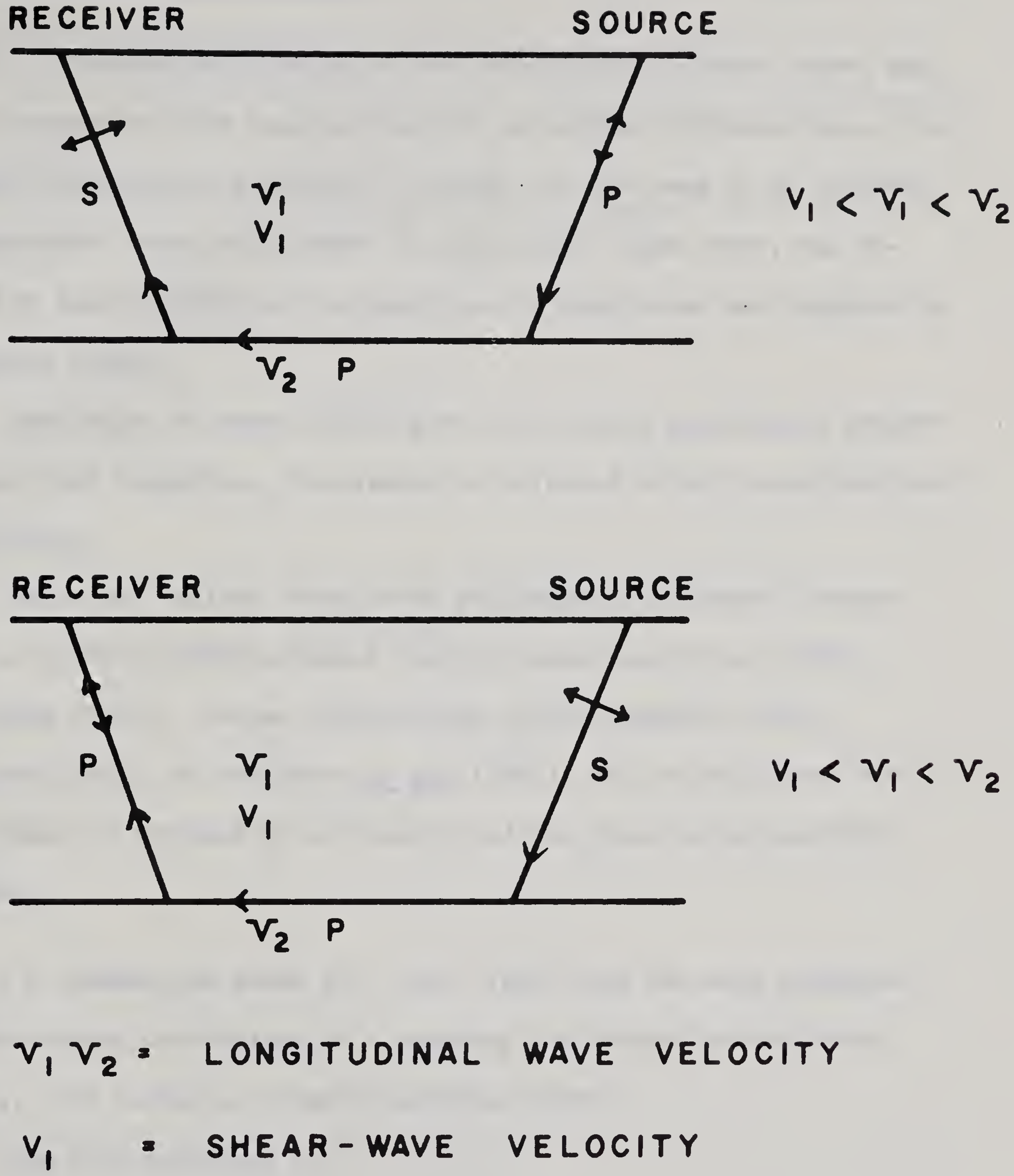
RECEIVER
SOURCE
S
v_1
V_1
P
$V_1 < v_1 < v_2$
v_2 P
RECEIVER
SOURCE
P
v_1
V_1
S
$V_1 < v_1 < v_2$
v_2 P
v_1 v_2 = LONGITUDINAL WAVE VELOCITY
V_1 = SHEAR-WAVE VELOCITY

Fig. II. 2

II. 2 Amplitude Relationships

II. 2. 1 Theoretical studies of the refraction of elastic waves and their conversion have been carried out in several different ways. For example the relative partition of energy for the case of an incident compressional wave or the same for an incident shear wave, was derived by Knott (1899) and the partition of amplitudes was expanded by Zoeppritz (1919).

Macelwane and Sohon (1932) give the various expressions derived by Knott and Zoeppritz. The reader is referred to this excellent work for details.

There are various other works published by different authors such as Jeffreys (1926), Muskat (1933), Muskat and Meres (1940), Gutenberg (1944), Heelan (1953), Nafe (1957), Schwind (1960), Richards (1961) and Steinhart et al. (1961), all of which deal with amplitudes of incident P- or S-waves and the other waves generated by them.

II. 2. 2 Muskat and Meres (oc. cit.) start with the wave equations of the various conversions at a boundary and deduce the amplitude ratios. The method is briefly described below.

The wave equations are

$$(\nabla^2 + h^2)\Phi = 0 \qquad h^2 = w^2/\alpha^2$$

where

$$(\nabla^2 + k^2)\Psi = 0 \qquad k^2 = w^2/\beta^2$$

w being the wave frequency and α and β the longitudinal and transverse wave velocities respectively.

For an incident longitudinal wave, they give the following system of equations.

$$\Phi_1 = I_1 e^{i(a_1 z - bx)} + R_1 e^{i(-a_1 z - bx)}$$

$$\Psi_1 = iS_1 e^{i(a_2 z - bx)}$$

$$\Phi_2 = I_2 e^{i(a_2 z - bx)}$$

$$\Psi_2 = iT_2 e^{i(c_2 z - bx)}$$

For an incident transverse wave the following relations hold.

$$\Phi_1 = R_1 e^{i(-a\ z - bx)}$$

$$\Psi_1 = iT_1 e^{i(c_1 z - bx)} + iS_1 e^{i(-c_1 z - bx)}$$

$$\Phi_2 = I_2 e^{i(a_2 z - bx)}$$

$$\Psi_2 = iT_2 e^{i(c_2 z - bx)}$$

where

$$a^2 + b^2 = h^2$$

$$c^2 + b^2 = k^2$$

$$b_1 = b_2 = b = \frac{w \sin \theta}{\alpha_1}$$

In Fig. II. 3 are shown these two cases when the incident wave

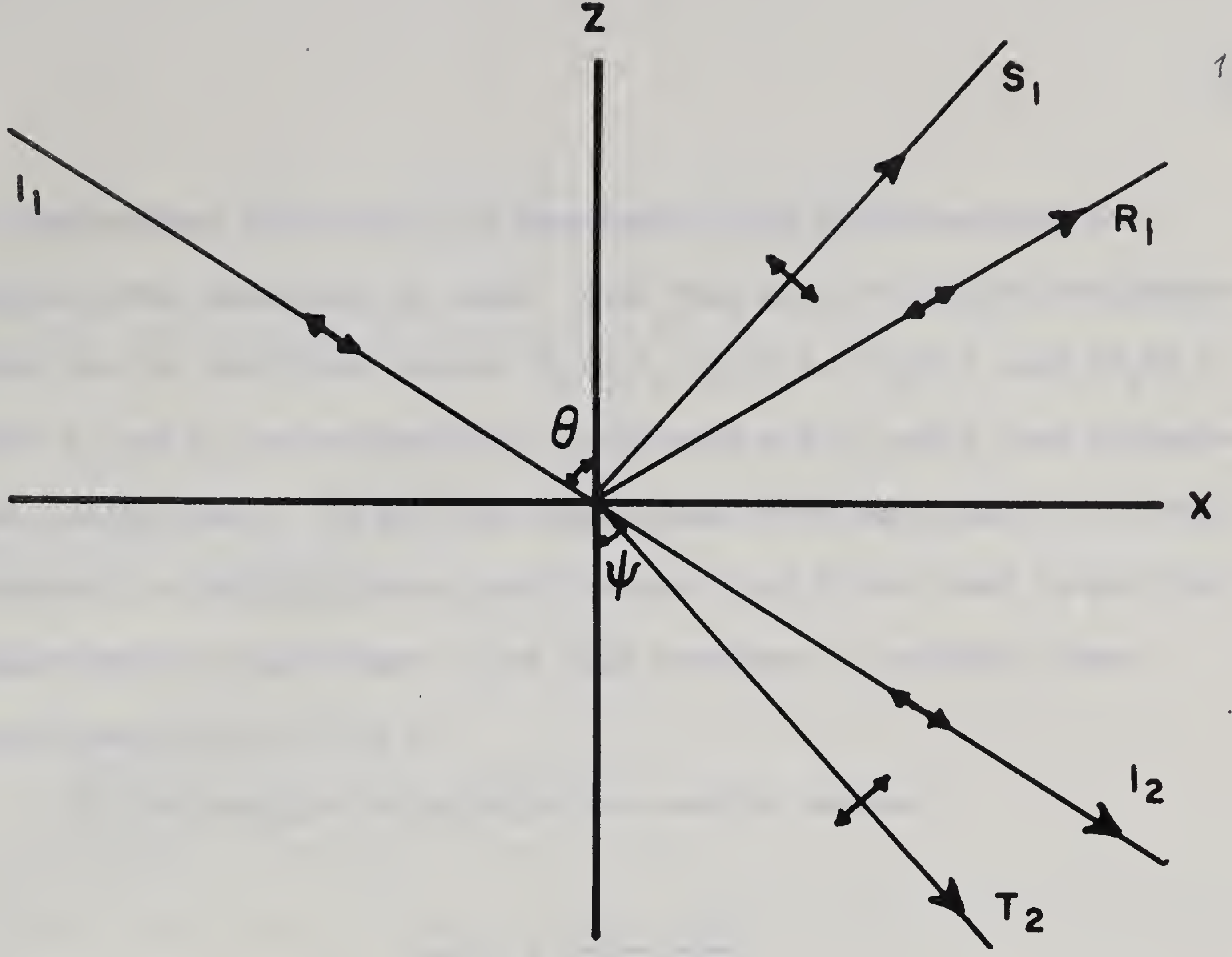

INCIDENT LONGITUDINAL WAVE

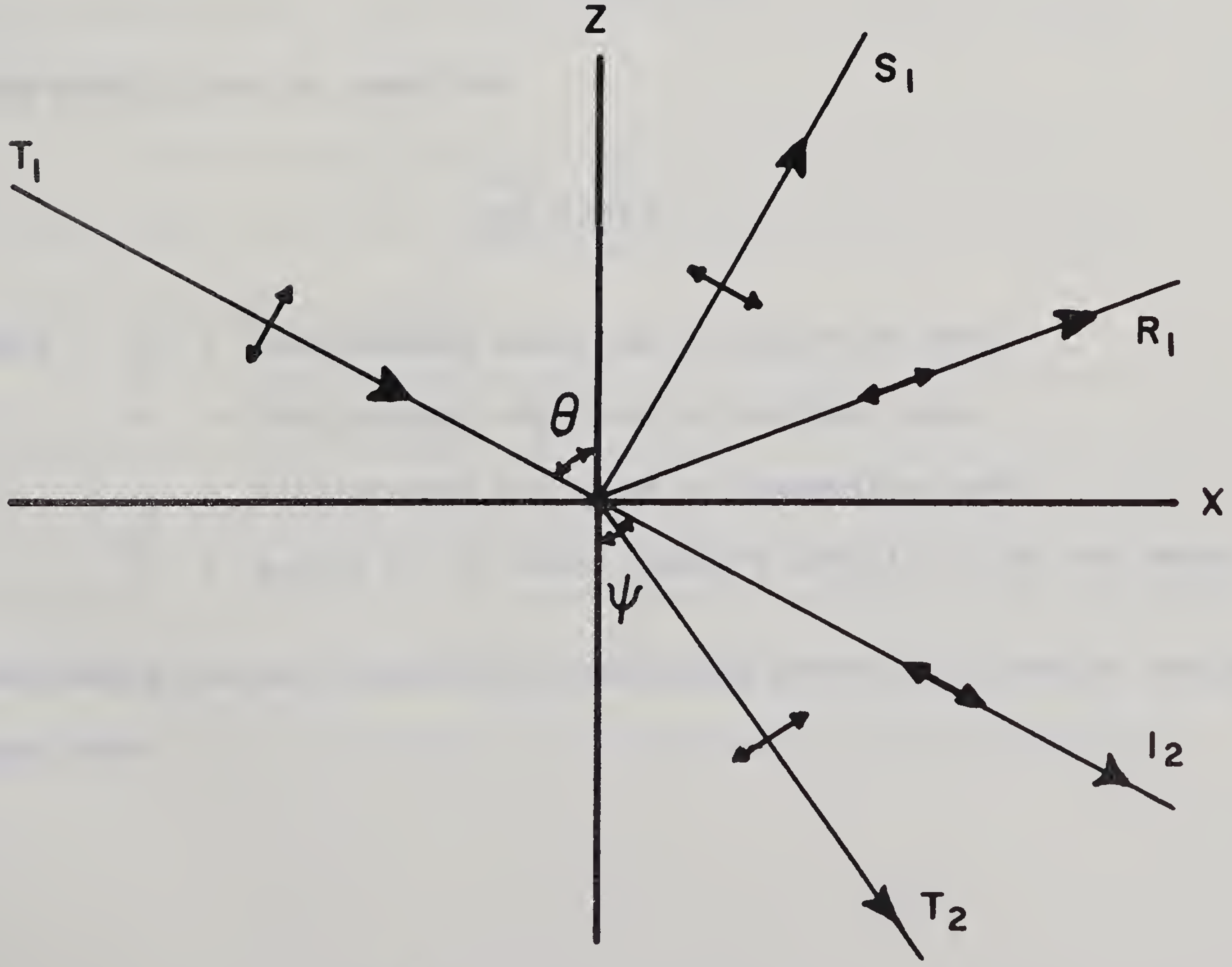

INCIDENT TRANSVERSE WAVE

Fig. II. 3

is longitudinal and when it is transverse, and also shown are the various waves generated by them. Then they go on to derive the expressions for the amplitude ratios (R_1/T_1), (S_1/T_1), (I_2/T_1), and (T_2/T_1) where R_1 and S_1 are reflection coefficients and I_2 and T_2 are transmission coefficients. To get the longitudinal wave amplitudes it is only necessary to multiply these coefficients (I or R) by h and to get the transverse wave amplitudes it is only necessary to multiply these coefficients (S or T) by k.

The following relationships are readily derived.

$$v_r/v_1 = \frac{(c_1 - c_2\delta)}{(c_1 + c_2\delta)}$$

$$v_2/v_1 = \frac{2c_1}{(c_1 + c_2\delta)}$$

From which it can be seen that

$$\frac{v_2}{v_1} = \frac{v_r}{v_1} + 1$$

where v_r → displacement amplitude of reflected wave

v_1 → displacement amplitude of incident wave

v_2 → displacement amplitude of transmitted wave

δ → μ_2/μ_1 ; μ_2, μ_1 being rigidity modulii of the two media.

Considering the wave intensities and energy partition it can be easily shown that

$$\frac{v_r^2}{v_1^2} = \left[\frac{1 - \bar{\beta}\bar{\gamma}\ \sqrt{\left(\bar{\beta}^2 + (1 - \bar{\beta}^2)\ \sec^2\theta\right)}}{1 + \bar{\beta}\bar{\gamma}\ \sqrt{\left(\bar{\beta}^2 + (1 - \bar{\beta}^2)\ \sec^2\theta\right)}}\right]^2$$

and hence the transmission coefficient is

$$\left(1 - \frac{v_r^2}{v_1^2}\right)$$

In the above expression

$$\bar{\beta} = \beta_2/\beta_1$$

$$\bar{\gamma} = \gamma_2/\gamma_1$$

γ_1, γ_2 are the densities of two layers.

β_1, β_2 are wave velocities in these layers.

In case of head waves the angle becomes critical angle which can now be given as

$$\text{Sin}\ \theta = \text{Sin}\ i_c = \frac{\alpha_1}{\alpha_2} = \frac{\beta_1}{\beta_2} \quad \text{for all} \quad \begin{matrix} \alpha_2 > \alpha_1 \\ \beta_2 > \beta_1 \end{matrix}$$

Muskat and Meres (op. cit.) have also published numerical results.

II. 2. 3 Heelan (1953) gives an erudite and elaborate treatment on the head waves, and on the incident P-waves and S-waves, and the conversions occurring thereby.

Heelan's argument starts almost at the same place where we ended the section 1 of this chapter. He recognizes a localized disturbance in the upper medium radiating P, SV and SH waves. When these waves are incident on the interface several systems of head waves and second order boundary waves are generated, each associated with grazing incidence of one or the other of the reflected or refracted waves.

Associated with the grazing incidence of P_1P_2, the refracted P-wave, is the head wave system comprising $P_1P_2P_1$, $P_1P_2S_1$ in the upper medium and $P_1P_2S_2$ in the lower medium. Associated with the grazing incidence of SV- disturbance are $S_1P_2P_1$, $S_1P_2S_1$ in the upper medium and $S_1P_2S_2$ in the lower medium. Either set of the three waves, mentioned above, satisfy the conditions of continuity of displacement and stress across the boundary.

The primary incident radiation generated by the source has the form of three auxiliary wave functions

$$\Phi_0 = \int_0^\infty e^{ikVt} \, dk \int_c f_0 H_0^{(1)}(\sigma r) e^{\alpha(z-d)} \, d\sigma$$

for longitudinal incident wave

$$\Theta_0 = \int_0^\infty e^{ikVt} \, dk \int_c g_0 H_0^{(1)}(\sigma r) e^{\beta(z-d)} \, d\sigma$$

for incident SV wave

and $$\chi_0 = \int_0^\infty e^{ikVt} \, dk \int_c n_0 H_0^{(1)}(\sigma r)^{\beta(z-d)} \, d\sigma$$

for incident SH-wave

where $$\alpha = \sqrt{\sigma^2 - k^2}$$

$$\beta = \sqrt{\sigma^2 - h^2}$$

$kV = h\nu$ and c is a loop $(\infty i, -k, -h, \infty i)$

where arg. σ = arg. α = arg. $\beta = \pi/2$ initially, and $2\pi \geqslant \arg. \sigma \geqslant 0$

on the path,

$$f_o = P_1(k)\Delta\sigma(2\sigma^2/h^2 + 1 - 2v^2/V^2)/8\pi\mu(\sigma^2 - k^2)^{1/2}$$

$$g_o = P_1(k)\Delta\sigma/4\pi\mu h^2$$

$$n_o = S_1(k)\Delta\sigma/4\pi\mu(\sigma^2 - h^2)^{1/2}$$

where $$P_1(t) = R\ell \int_{0\infty}^{\infty} P_1(k)\exp(ikVt)dk$$

$$S_1(t) = R\ell \int_{0}^{\infty} S_1(k)\exp(ikVt)dk$$

$R\ell$ indicating the real part of the integrals.

Δ = volume of the cylindrical source

μ = rigidity of the medium

V, v = velocities of P and S waves respectively.

Heelan then lets Φ, Θ and χ satisfy the well known wave equations, and expresses three functions for both media in the integral form shown above. Applying the boundary conditions, of continuity of displacements and stresses, he arrives at six linear equations and solves them for functions f_1, g_1, n_1, f^1, g^1, n^1.

He then derives the integral expressions for vertical and horizontal displacements for PP, SP, PS, SS and other wave types, and then solves them for vertical and horizontal displacements for $P_1P_2P_1$, $P_1P_2S_1$ and $P_1P_2S_2$. These expressions could be evaluated numerically and compared with experimental data.

II. 3 Travel-Time Relationships

Scwhind et al. (1960) determine the crustal layering by using PS converted phases and the picture obtained thereby, at the sites mentioned in their paper, favorably compares with that given by other methods.

II. 3. 1 For an n-layer model the equation for a wave travelling throughout as a P-wave as in figure II. 4 is given by Hall (op. cit.)

$$T = \frac{x}{V_n} + \sum_{i=1}^{n-1} \eta(V_i, V_n)(h_i + h_i')$$

where x is the distance between shot point and detector

h_i is the thickness of ${}_i$th layer under detector

h_i' is the thickness of ${}_i$th layer under shot point

V_i is the compressional wave velocity in ${}_i$th layer

and $$\eta(u_i, u_j) = \sqrt{\frac{1}{u_i^2} - \frac{1}{u_j^2}} = \frac{1}{u_i}\sqrt{1 - \frac{u_i^2}{u_j^2}} = \frac{\text{Cos } i_{c_{i,j}}}{u_i}$$

$$\text{for all } u_i < u_j$$

If the conversion has taken place in ${}_j$th layer then the expression V_j in $\eta(V_j, V_n)$ is simply changed to v_j, indicating the conversion of compressional wave to shear wave where v_j is the shear wave velocity in ${}_j$th layer. The same thing is done if there are more than one conversion. This is true for the case for beds with small dip; if the dip is severe then a dip factor enters into calculation.

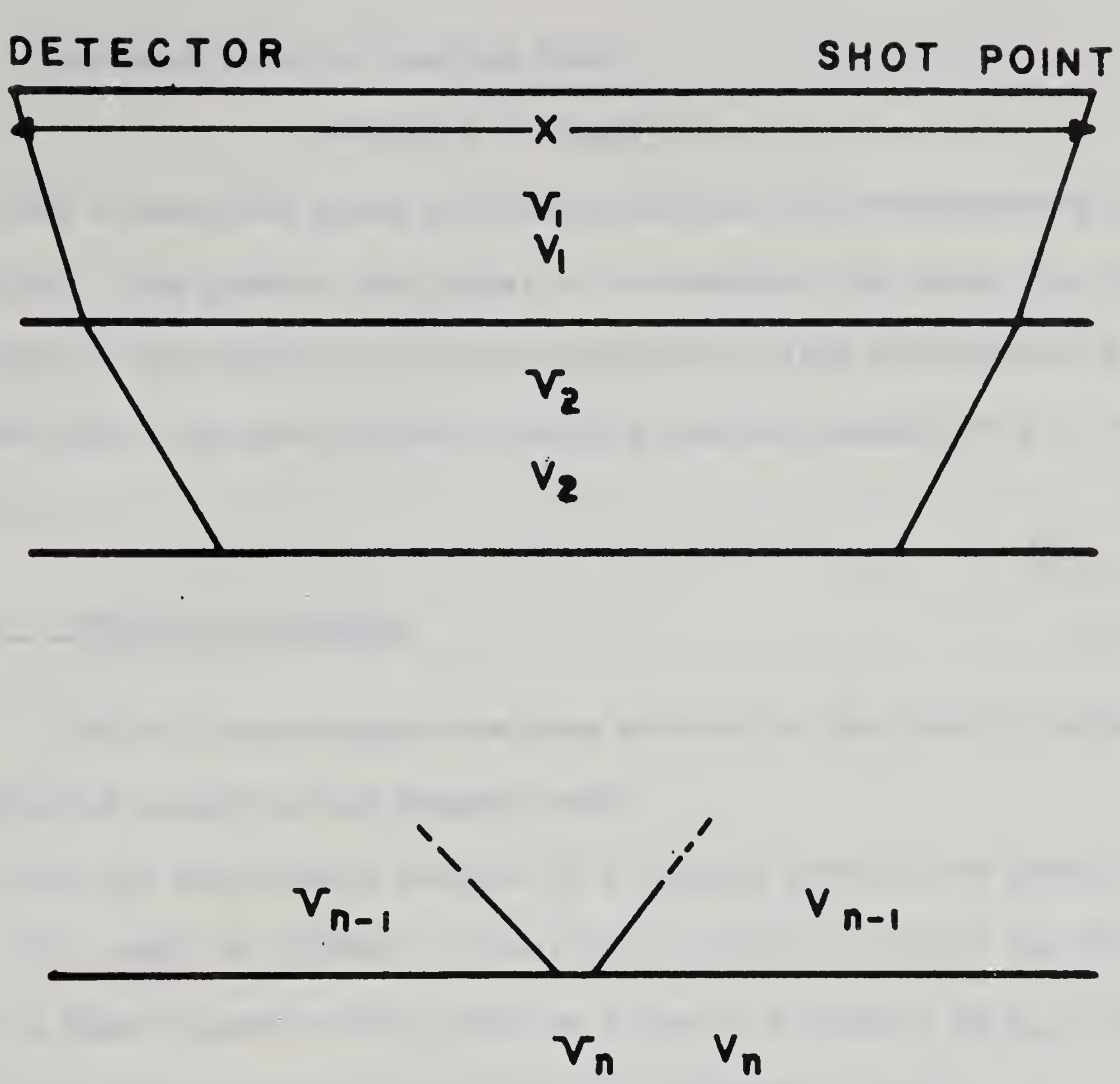

N - LAYERED MODEL

$\mathcal{V}_1$ --- $\mathcal{V}_n$ = P WAVE VELOCITIES

V_1 --- V_n = S WAVE VELOCITIES

Fig. II. 4

Mathematically we can see that

$$\eta(v_i,V_j) > \eta(V_i,V_j)$$

so that a converted phase arrives later than the corresponding P arrival. The greater the number of conversions the later the event arrives. Physically it is much more clear, since the converted phase takes more time than the corresponding P-event because of its lower velocity.

II. 4 Method of Analysis

The following scheme has been adopted in the identification of converted phases in the present work.

1. All the events were plotted on a reduced travel time graph $(T - \frac{x}{6.5})$ VS DISTANCE. (Fig. III. 1, III. 3, III. 4 and III. 7)
2. A least square method, such as given by Steinhart et al. (1961), was applied to get velocities and intercept times.
3. Based on this velocity model along with the well information on sediments at the shot sites, intercept times for various converted phases were calculated.
4. Whenever these times showed a reasonable agreement with the intercept times in step 3., the event has been identified as that particular event.
5. The phase relationship of the suspected converted phase was such as to indicate a clear SV-motion. This was sometimes not true. (Fig. III. 8a)

6. An amplitude measurement was made for the later events and compared with compressional wave arrival. (Fig. III. 9a and 9b)
7. A qualitative comparison of frequencies were also made. (Fig. II. 5a, 5b, 5c)
8. A few particle motion diagrams were constructed where the data were of high enough quality. (Fig. III. 8a, 8b, 8c)

It can be clearly seen that the time difference between compressional wave arrival and converted phase arrival gives the information about the thickness of the layer in which conversion has taken place. This is one great advantage working with these phases. No information about the exact location of shot point or exact time of shot occurrence is needed to derive the picture of layering. For gently dipping beds, the dip could be easily calculated by solving the different equations involved for depths under detector and shot point. Theoretically, at least, it is always possible to find converted phases which give information about these two quantities for a particular layer. In the case of deep curvature of the beds, as already mentioned, a dip factor enters into calculations.

II. 4.a. Some of the criteria mentioned in the identification of converted phases are shown in a few records reproduced here. (Fig. II. 5a, 5b, 5c) In fig. II. 5b are shown the first arrival (T_1) from Moho and a Moho conversion (T_3). The horizontal component traces are indicated by Radial and Transverse and the vertical component is

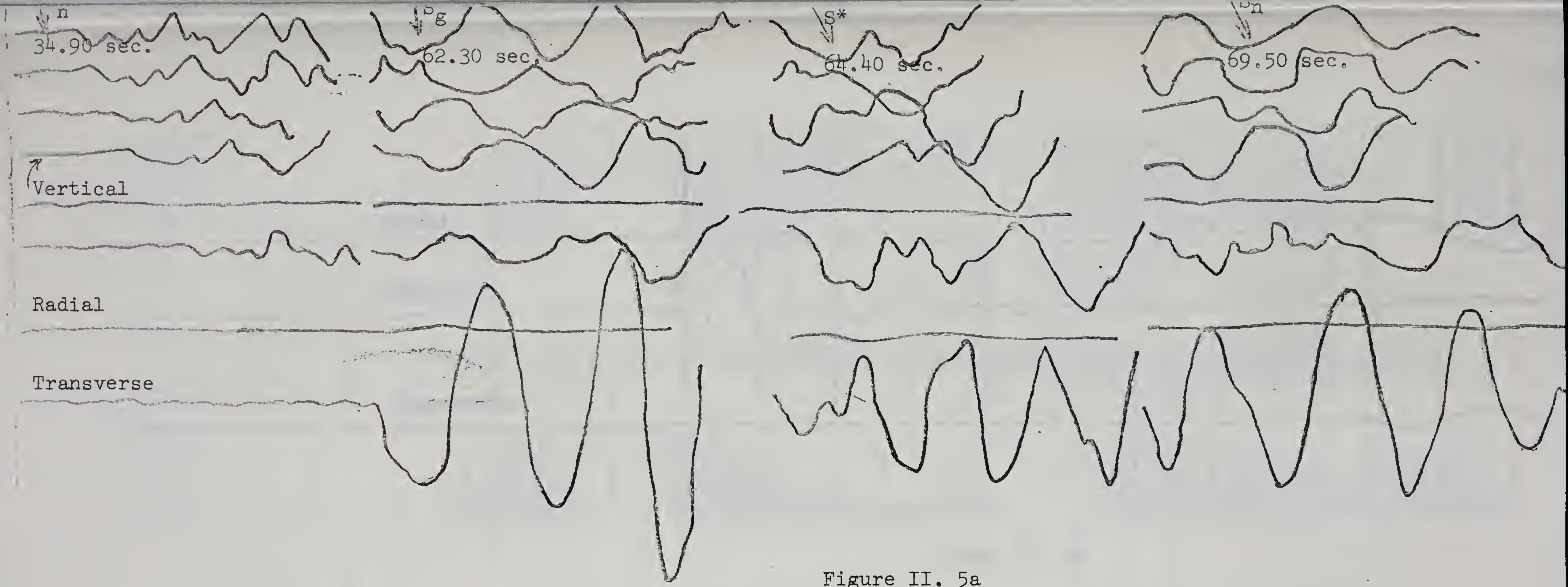

Figure II. 5a

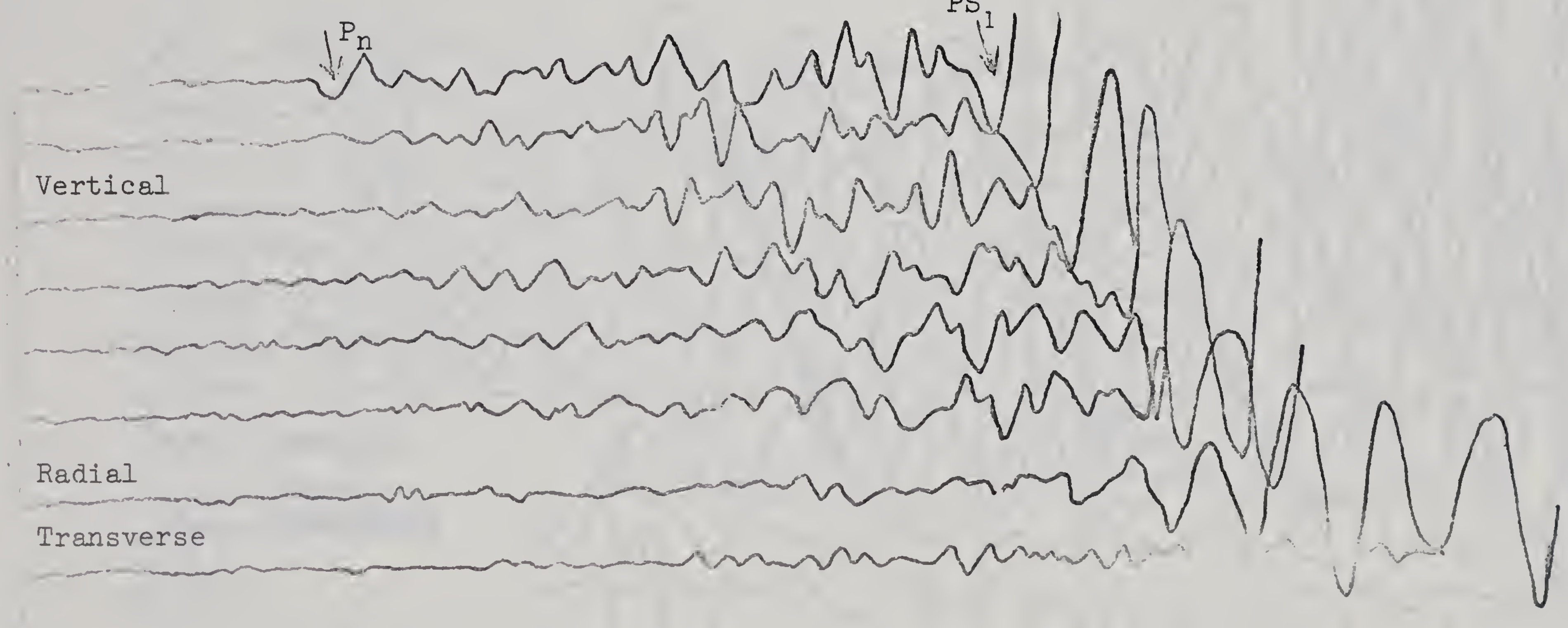

Figure II. 5b

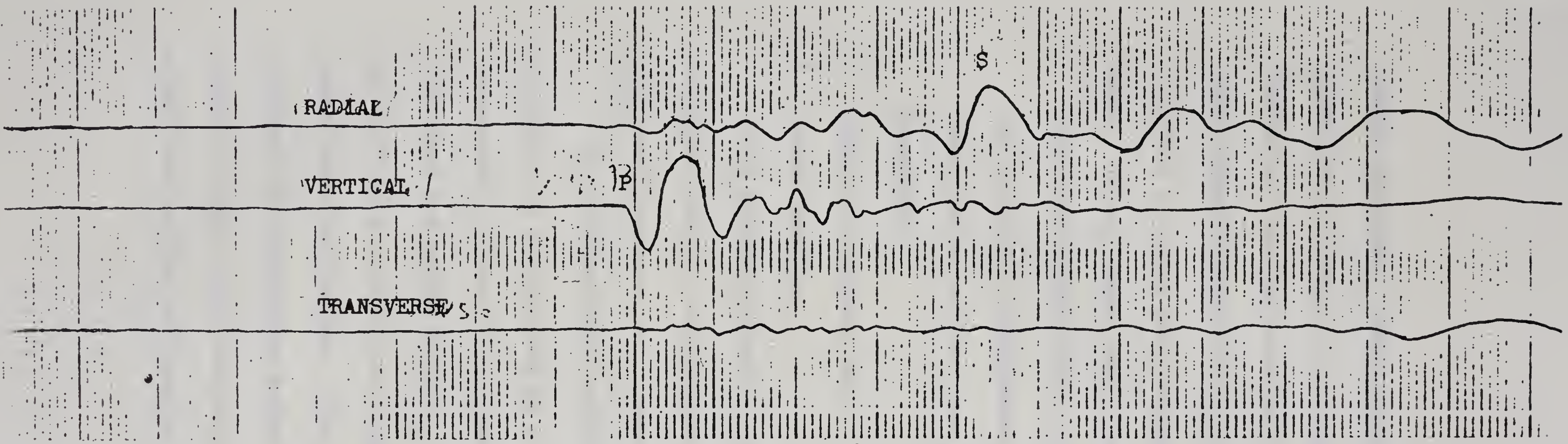

Figure II. 5c

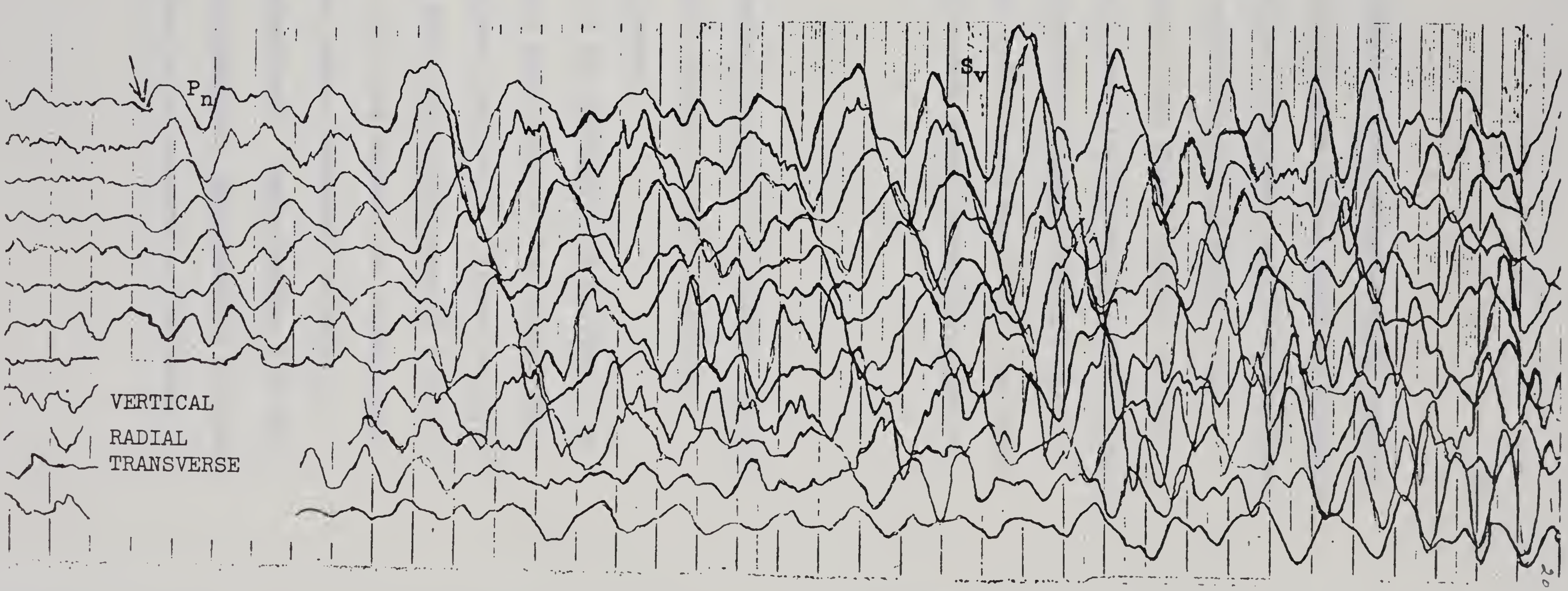

Figure II. 5d

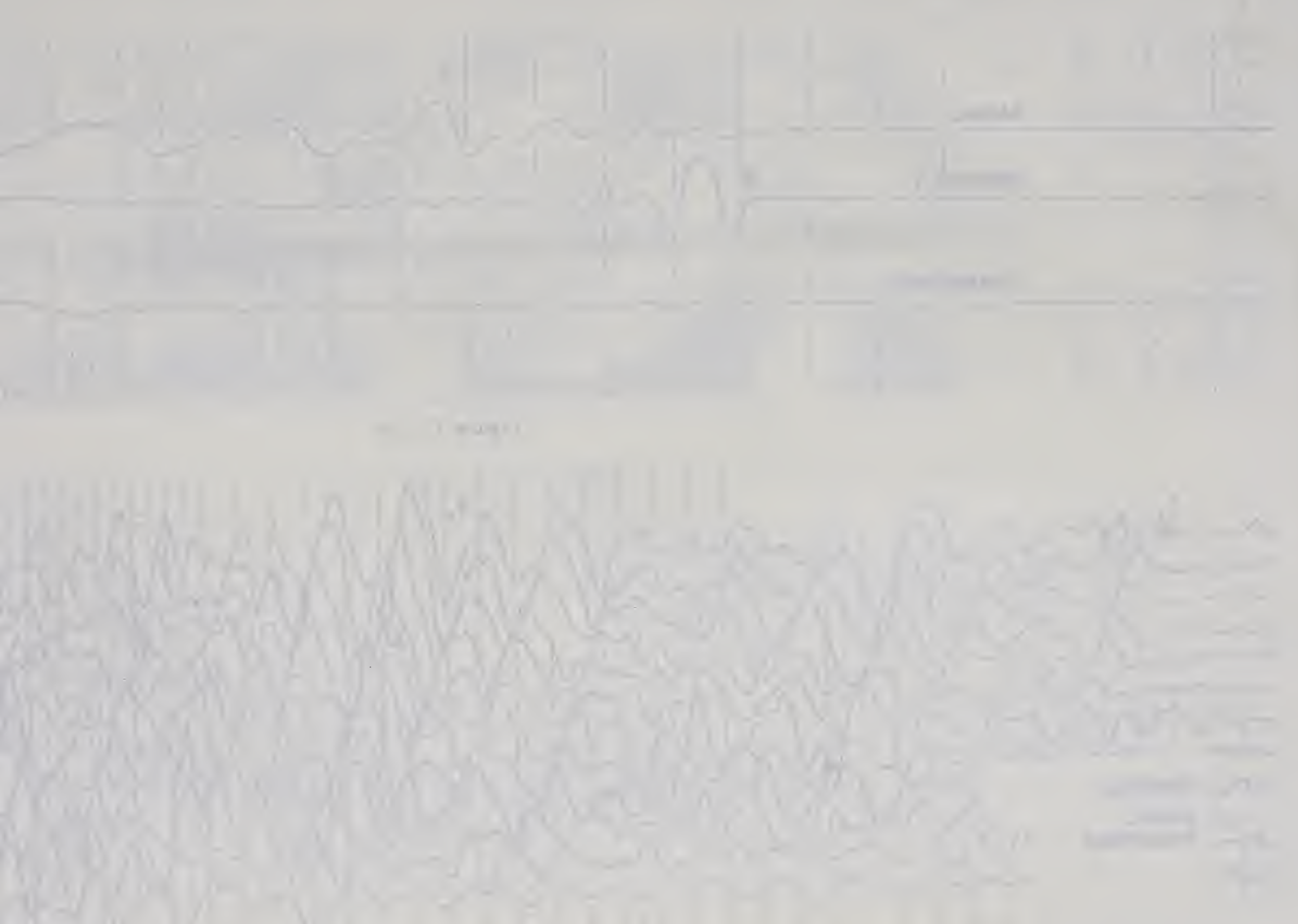

denoted as shown. Radial motion can be clearly observed on PS_1 showing S_V-motion. In fig. II. 5d clear S_V-motion is marked along with P-motion, whereas in fig. 5a S-arrivals from the subbasement and the intermediate layer respectively at 62.30 sec. and 64.40 sec. are shown. The S-arrival at 69.50 sec. corresponds to Moho whose P-arrival is also shown. In all these cases one can observe the following characteristics.

1. Large horizontal motion (On S-arrival, a large transverse motion can be seen. Unfortunately the radial trace was dead. The transverse motion with a clear well marked spread velocity points to S_H-motion.)
2. Larger amplitudes, and
3. Longer periods.

The second criterion was however not true in all cases. But it conforms with the observation made by Andreev (loc.cit) that the amplitude increases for converted phases.

The observational evidence for the generation of S_V-wave by an explosion is illustrated by a record shown here in fig. II.5c. This is a record of the 500 ton surface shot taken at a distance of 10,000 feet from the charge centre. The shot time is indicated by a dot on the left hand side of the figure. The time between two consecutive thick lines is 0.20 sec. The three traces represent the radial, vertical and transverse motion respectively. Approximately 1.20 sec. after the shot, the P-motion can be observed. Approximately 0.90 sec. after this motion the S_V-type motion can be observed on the radial

trace. This represents the conversion of P to S very near the shot point and indicates that for this shot at least it should be possible to observe events at large distances, which have the first part of their path as S_V type motion.

CHAPTER III

EXPERIMENTAL RESULTS

III. 1 Records examined for the purpose of the present work belong to two profiles as already mentioned.

1. Bow City West. The shot point was at Bow City, and the recording sites west of Bow City covering a profile of about 180 kilometres. There were fourteen records obtained on this profile.
2. Suffield West. The shot point was at Suffield, and the recording sites were to the west, covering a total distance of about 520 kilometers. Only that part of the profile beyond about 216 kilometers is studied here, consisting of ten records from the 500 ton shot. The locations of these profiles are indicated on fig. I. 1.

III. 2 First Arrivals From Bow City

Fig. III. 1 is the reduced travel time graph of various events identified on the Bow City records.

The spread velocity for first arrivals on this profile is 6.16 km/sec for the first seven records and 6.50 km/sec for the rest of the records. On two records the first arrivals could not be identified with any confidence but immediately following is an arrival with 6.50 km/sec velocity. The two horizons represented by these arrivals are respectively referred to as the Basement (6.16 km/sec) and the Sub-

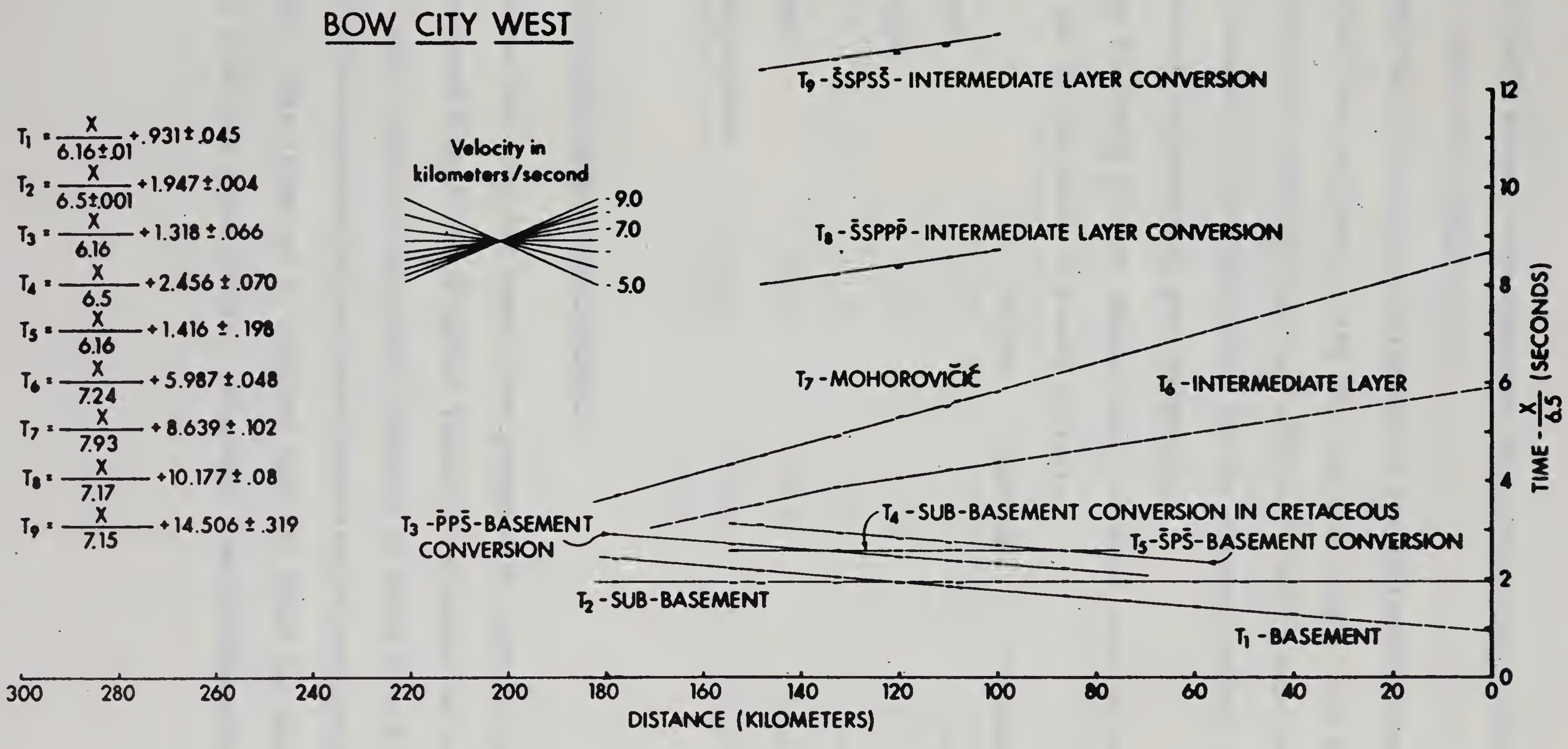
BOW CITY WEST
$T_1 = \frac{X}{6.16 \pm .01} + .931 \pm .045$
$T_2 = \frac{X}{6.5 \pm .001} + 1.947 \pm .004$
$T_3 = \frac{X}{6.16} + 1.318 \pm .066$
$T_4 = \frac{X}{6.5} + 2.456 \pm .070$
$T_5 = \frac{X}{6.16} + 1.416 \pm .198$
$T_6 = \frac{X}{7.24} + 5.987 \pm .048$
$T_7 = \frac{X}{7.93} + 8.639 \pm .102$
$T_8 = \frac{X}{7.17} + 10.177 \pm .08$
$T_9 = \frac{X}{7.15} + 14.506 \pm .319$
Velocity in kilometers/second
9.0
7.0
5.0
T_9 - $\bar{S}SPS\bar{S}$ - INTERMEDIATE LAYER CONVERSION
T_8 - $\bar{S}SPP\bar{P}$ - INTERMEDIATE LAYER CONVERSION
T_7 - MOHOROVIČIĆ
T_6 - INTERMEDIATE LAYER
T_4 - SUB-BASEMENT CONVERSION IN CRETACEOUS
T_5 - $\bar{S}P\bar{S}$ - BASEMENT CONVERSION
T_3 - $\bar{P}P\bar{S}$ - BASEMENT CONVERSION
T_2 - SUB-BASEMENT
T_1 - BASEMENT
TIME - $\frac{X}{6.5}$ (SECONDS)
12
10
8
6
4
2
0
300
280
260
240
220
200
180
160
140
120
100
80
60
40
20
0
DISTANCE (KILOMETERS)

Fig. III. 1

basement (6.50 km/sec) with intercept times of (0.931 ± 0.045) sec. and (1.947 ± .004) sec. respectively.

From the well data the thickness of the sedimentary layers and their velocities are known at the Bow City Shot Point. The theoretically calculated intercept time is 0.870 sec. Taking into account both the uncertainties in the calculated and the observed values, this is considered to be reasonably good agreement.

The following picture emerges when the depth calculations are carried out on the basis of P-wave arrivals.

	Vel. km/sec.	Depth km.	Thickness km.
Cretaceous	3.41		1.40
Mississipian	5.80	1.40	1.10
Basement	6.16	2.50	9.77
Subbasement	6.50	12.27	23.16
Intermediate Layer	7.25	35.43	13.27
Moho	7.93	48.70	

III. 3 Converted Phases from Basement

One can see from the travel time graphs that there are two very well correlated events with a spread velocity corresponding to 6.16 km/sec. Larger amplitude and lower frequency of these events point to some sort of an S-motion but the spread velocity is characteristically P-velocity. This leads one to conclude that the event has been converted to S at some upper levels. Intercept time considerations show

that the conversion has taken place in the sedimentary layers as shown in fig. III. 2. Thus the above two events have been identified as PPPPS and PPPSS. The equations governing the two events are given below.

$$T_3 = \frac{x}{V_3} + \eta(V_1',V_3)h_1' + \eta(V_2',V_3)h_2' + \eta(v_1,V_3)h_1 + \eta(V_2,V_3)h_2 \tag{1}$$

$$T_5 = \frac{x}{V_3} + \eta(V_1',V_3)h_1' + \eta(V_2',V_3)h_2' + \eta(v_1,V_3)h_1 + \eta(v_1,V_3)h_2 \tag{2}$$

where	T	is the time taken by the ray to travel from shot point to detector location.
	h_1',h_2'	are thicknesses of the layers under the shot point.
	h_1,h_2	are thicknesses of the layers under the detectors.
	V_1,V_2,V_3	are P-wave velocities in the three layers
and	v_1,v_2	are S-wave velocities in the first two layers,

also $$\eta(U_i,U_j) = \sqrt{\frac{1}{U_i^2} - \frac{1}{U_j^2}} = \frac{1}{U_i}\sqrt{1 - \frac{U_i^2}{U_j^2}} = \frac{\text{Cos } i_{c_{i,j}}}{U_i}$$

where $\sin i_c = \frac{U_i}{U_j}$ for all $U_i < U_j$.

It is assumed that the following relationship holds between the P-wave and S-wave velocities in ith layer.

$$V_i = \sqrt{3}\, v_i$$

The ray path for P-motion in the above structure is given by

$$T_1 = \frac{x}{V_3} + \eta(V_1,V_3)h_1 + \eta(V_1',V_3)h_1' + \eta(V_2',V_3)h_2' + \eta(V_2,V_3)h_2 \tag{3}$$

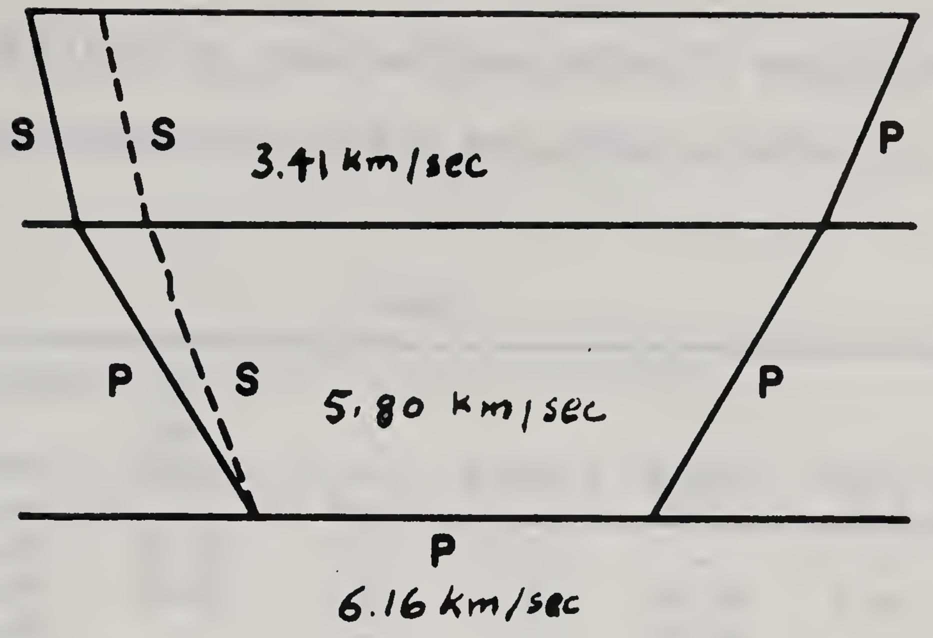

Fig. III. 2

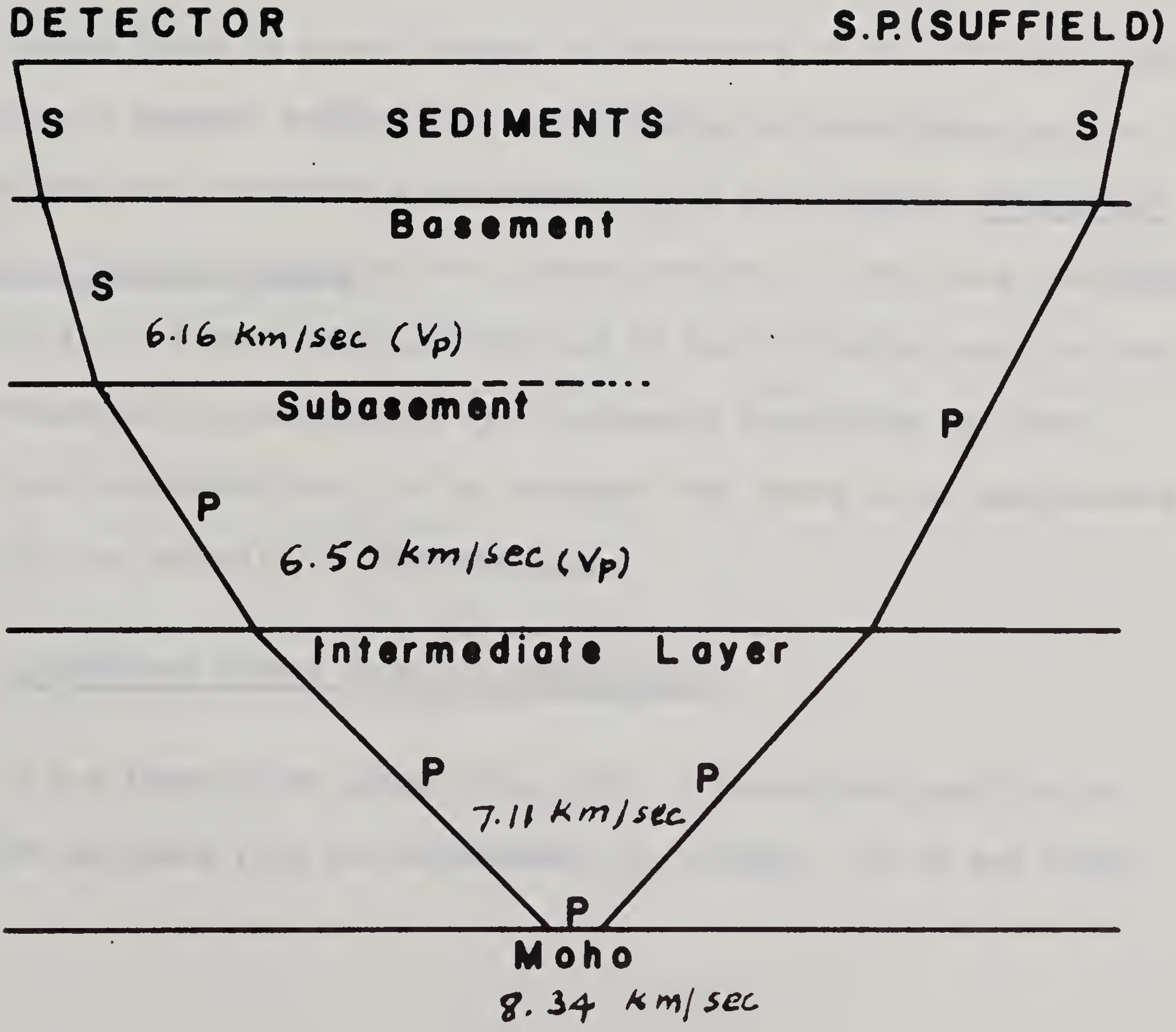

Fig. III. 5

Solving (1) and (3) for h_1, one can then solve (1) and (2) for h_2. The estimates of the values of h_1 and h_2 are given in Table 1.

TABLE 1

x(km.)	T_1(secs) PPPPP	T_2 sec PPPPS	T_2-T_1 sec	h_1(km.)	T_3 PPPSS sec	T_3-T_2 sec	h_2(km.)
176.96	29.65	30.22	0.57	2.71	-	-	-
153.59	25.84	26.38	0.54	2.57	26.88	0.50	2.63
148.46	25.04	-	-	-	25.98	-	-
132.23	22.39	-	-	-	23.29	-	-
120.06	20.42	20.92	0.50	2.38	21.31	0.39	2.05
110.07	18.74	19.28	0.54	2.57	19.68	0.40	2.11
108.14	18.46	18.94	0.48	2.29	19.36	0.42	2.21
100.38	-	17.69	-	-	18.12	-	-
86.17	14.91	15.41	0.50	2.38	15.61	0.20	1.05

Though there is a good amount of scattering in the estimation for h_1 and h_2, a general feature is the thickening of both layers as one goes to the west towards the mountains. (See for example Geological History of Western Canada by the Alberta Society of Petroleum Geologists.)

In all the above calculations and in the following ones the lateral variations in velocity in the Cretaceous formations has been taken into consideration. It was assumed that there is no appreciable change in the velocity in the Mississippian.

III. 4 Converted Phases from the Subbasement

On the travel time graph (Fig. III. 1) an arrival parallel to the first arrivals from the subbasement is evident. It is not fully

understood at what horizon this event originates. It seems to be a converted phase but the times are not consistent with a simple interpretation.

III. 5 Estimate of the Thickness of the Basement

Since the ray path travel time for P-motion from the subbasement is given by

$$T_2 = \frac{x}{V_4} + \eta(V_1',V_4)h_1' + \eta(V_1,V_4)h_1 + \eta(V_2',V_4)h_2' + \eta(V_2,V_4)h_2 + \eta(V_3,V_4)(h_3 + h_3') \qquad (4)$$

one can estimate the values for $(h_3 + h_3')$ at different distances. (4) can be written as

$$(h_3 + h_3') = \frac{T - \{\frac{x}{V_4} + \eta(V_1',V_4)h_1 + \eta(V_2',V_4)h_2' + \eta(V_2,V_4)h_2\}}{\eta(V_3,V_4)} \qquad (4a)$$

All the quantities on the right hand side of (4a) are known. We can now calculate $(h_3 + h_3')$ at different values of x. These are given in Table 2.

The scatter in values for $(h_3 + h_3')$ is not too high compared to the same in h_1, h_2. A general feature of interest is the thinning under the mountains of the layer with 6.16 km/sec. velocity.

Table 2

Bow City Arrivals from the Subbasement and their Interpretation

x Km	$T-\frac{x}{6.5}$ sec	$.194h_1$ sec	$.077h_2$ sec	T sec	h_3+h_3' Km	h_3 Km
176.96	1.95	.526	-	-	-	-
153.59	1.95	.499	.20	.814	18.08	8.31
148.46	1.95	-	-	-	-	-
132.23	1.95	-	-	-	-	-
120.06	1.95	.462	.158	.893	19.84	10.07
110.07	1.95	.499	.162	.842	18.71	8.94
108.14	1.95	.444	.170	.90	20.00	10.23
100.38	1.95	-	-	-	-	-
86.17	1.95	.462	.081	.97	21.56	11.79
					Average h_3 =	9.86

III. 6 Converted Phases from Intermediate Layer

Two events were identified with the same velocity as that of the intermediate layer. The correlation from record to record is good. On the basis of intercept times these two events, in the order of occurrence, have been respectively identified as

1. conversion in basement and sediments
2. conversion in basement and sediments, and conversion in subbasement only under the shot point.

Table 3 gives the estimations of thicknesses of various layers based on these conversions from the Intermediate Layer.

Table 3

Intermediate Layer Arrivals

	T_1	T_2				T_3		
x	PPPPP	SPPPS	T_2-T_1	h_3+h_3'	h_3	SSPPS	T_3-T_2	h_4'
Km	sec	sec	sec	Km	Km	sec	sec	Km
153.59	27.18	-	-	-	-	-	-	-
148.46	26.49	30.89	4.40	19.10	9.33	35.29	4.40	26.39
132.23	24.24	28.64	4.40	19.10	9.33	32.99	4.35	26.06
120.06	22.57	26.92	4.35	18.76	8.99	31.31	4.39	26.32
110.07	21.18	25.53	4.35	18.76	8.99	29.85	4.32	25.87
100.38	19.84	24.19	4.35	18.76	8.99	28.59	4.40	26.39
					Aver. = 9.13			Aver. = 26.20

The following picture emerges from these calculations.

Shot Point	Thickness km	Velocity km/sec.
*Cretaceous	1.4	3.47
*Mississippian	1.1	5.80
Basement	9.77	6.16
Subbasement	26.20	6.50
Detectors		
Cretaceous	2.48	4.01
Mississippian	2.00	5.80
Basement	9.13	6.16
Subbasement	20.95	6.50

There is an apparent discrepancy in the value for the subbase-

---

* From the well data.

ment thickness under the shot point as calculated in two different ways i.e. from first arrivals and from conversions from the intermediate layer. This is mainly due to the small quantities involved in the calculations for these converted phases. The times are small and the η's are small. A change even in third decimal place in η's causes a change of 3 - 4 km in thickness estimates.

III. 7 First Arrival Data From Suffield 500 Ton Profile

In fig. III. 3 and III. 4 are given the reduced travel-time graphs of some events observed on 500 ton records.

The first arrivals from 500 ton profile have a spread velocity of about 8.37 km/sec. The correlation from record to record is fairly satisfactory. The intercept time is 9.25 ± 0.14 sec. Following this event a number of other events were identified and plotted on the graph. The event with velocity 7.11 km/sec corresponding to the intermediate layer has an intercept time of 5.60 ± 0.12 sec. The following table gives the intercept times and velocities for both

Table 4

	Velocity Km/Sec.		Intercept Time Sec.	
	Moho	Inter Layer	Moho	Inter Layer
Bow City Profile	7.93 ± .05	7.24 ± .002	8.64 ± .10	5.99 ± .05
500 Ton Profile	8.37 ± .04	7.11 ± .004	9.25 ±0.14	5.60 ±0.12

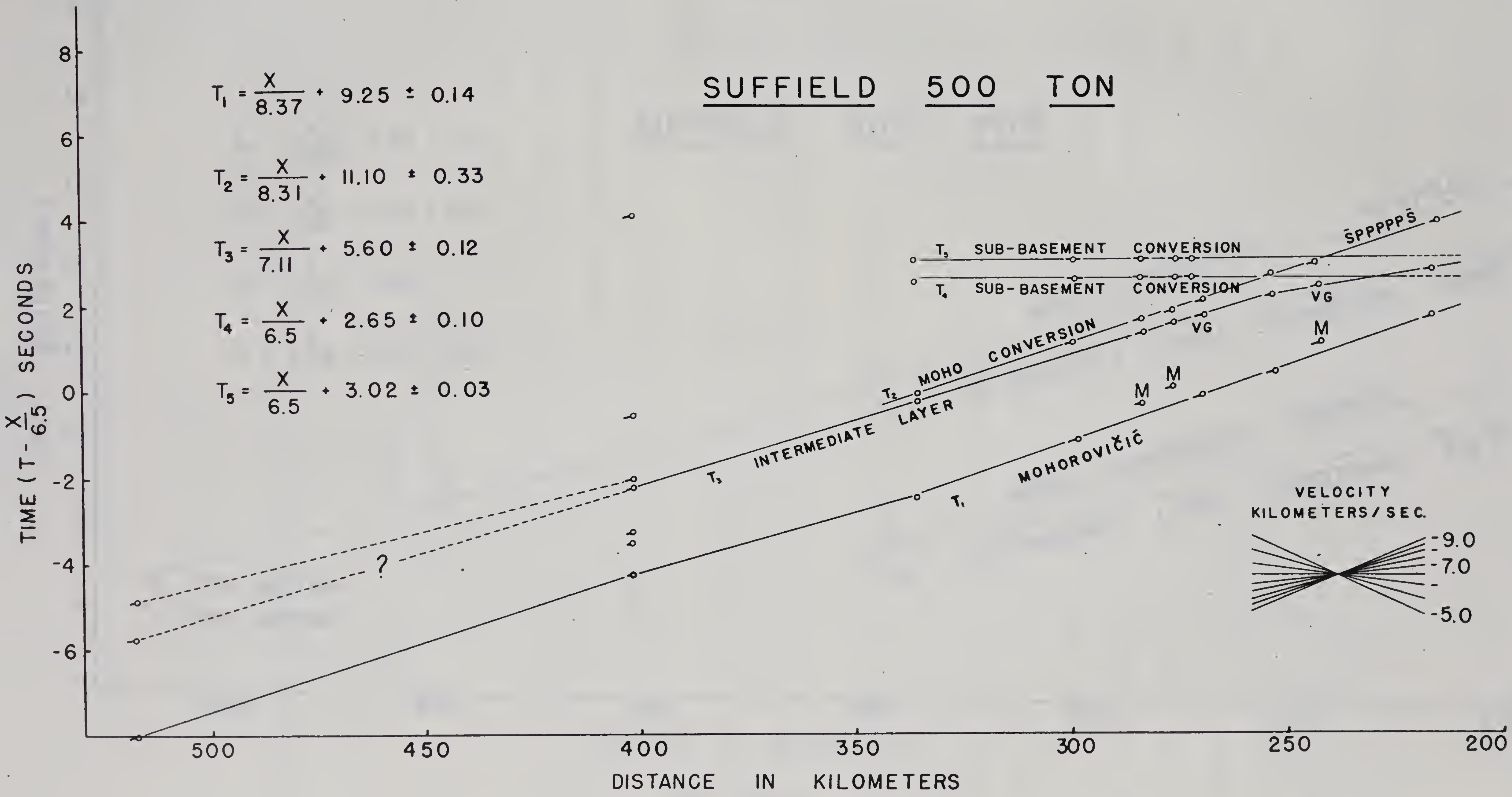
SUFFIELD 500 TON
$T_1 = \frac{X}{8.37} + 9.25 \pm 0.14$
$T_2 = \frac{X}{8.31} + 11.10 \pm 0.33$
$T_3 = \frac{X}{7.11} + 5.60 \pm 0.12$
$T_4 = \frac{X}{6.5} + 2.65 \pm 0.10$
$T_5 = \frac{X}{6.5} + 3.02 \pm 0.03$
T_3 SUB-BASEMENT CONVERSION
T_4 SUB-BASEMENT CONVERSION
$\bar{S}PPPPP\bar{S}$
T_2 MOHO CONVERSION
VG
VG
M
M
M
T_5 INTERMEDIATE LAYER
T_1 MOHOROVIČIĆ
?
VELOCITY
KILOMETERS/SEC.
9.0
7.0
5.0
TIME ($T - \frac{X}{6.5}$) SECONDS
8
6
4
2
0
-2
-4
-6
500
450
400
350
300
250
200
DISTANCE IN KILOMETERS

Fig. III. 3


HOT DOG DIAGRAM

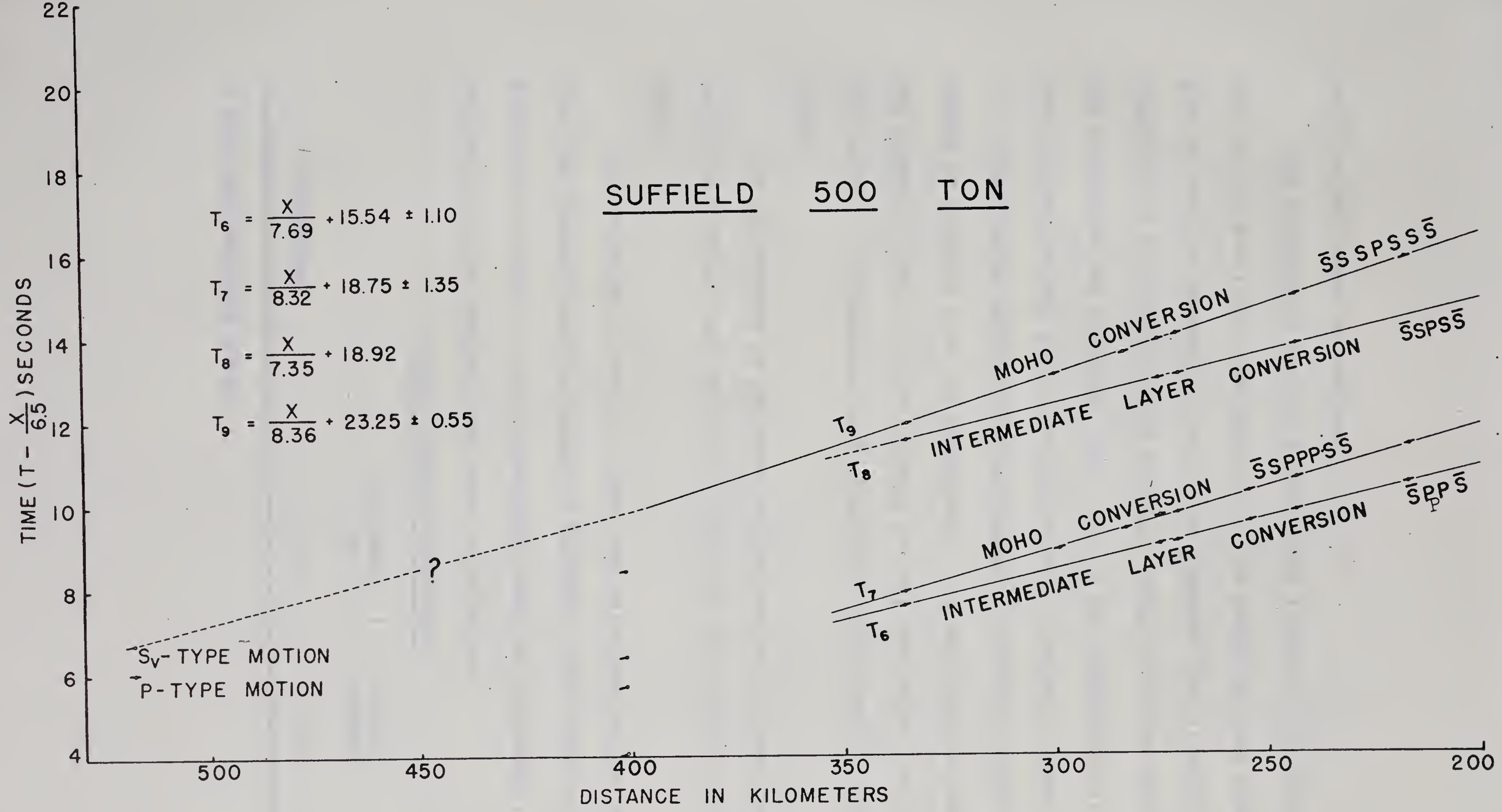
SUFFIELD 500 TON
$T_6 = \frac{X}{7.69} + 15.54 \pm 1.10$
$T_7 = \frac{X}{8.32} + 18.75 \pm 1.35$
$T_8 = \frac{X}{7.35} + 18.92$
$T_9 = \frac{X}{8.36} + 23.25 \pm 0.55$
MOHO CONVERSION
INTERMEDIATE LAYER CONVERSION
MOHO CONVERSION
INTERMEDIATE LAYER CONVERSION
$\bar{S}SSPSS\bar{S}$
$\bar{S}SPS\bar{S}$
$\bar{S}SPPPS\bar{S}$
$\bar{S}P_PS\bar{S}$
T_9
T_8
T_7
T_6
?
S_V- TYPE MOTION
P- TYPE MOTION
TIME $(T - \frac{X}{6.5})$ SECONDS
4
6
8
10
12
14
16
18
20
22
DISTANCE IN KILOMETERS
500
450
400
350
300
250
200

Fig. III. 4

profiles for these two horizons.

The correlation for the intermediate layer for the 500 ton profile is not good, with the result that the event has been shown on the plot by two line segments. One of the segments fits in with the remainder of the Suffield West profile. These two lines have different velocities and intercept times, and if the correlation is correct, they indicate strong dip on the top of the 7.1 km/sec. layer.

There is no arrival from the basement. However, there are a number of arrivals from the subbasement. It was therefore assumed that the basement layer is either missing or very thin under the Suffield shot point, a circumstance to be confirmed later from the converted phases.

The thicknesses of sediments and velocities in these formations under the Suffield shot point are known with fair accuracy from well data.

The thickness of the 6.50 layer was calculated on the assumption that the basement layer is absent at Suffield. The value is 31.50 km. Similarly the depth to the intermediate layer was calculated. The following picture emerges from these calculations.

Under Suffield Shot Point

	Thickness km	Velocity km/sec.
*Cretaceous	1.30	2.11

---

* From well velocity survey

	Thickness km	Velocity km/sec.
*Mississippian	0.84	5.80
Subbasement	31.50	6.50
Intermediate Layer	10.00	7.11

Depth to Moho 43.64 km.

Velocity below Moho 8.34 km/sec.

III. 8 Converted Phases from the Mohorovicić

The first of these phases occurs just about 2.30 seconds after the first arrival. This has been identified on the basis of intercept times as the conversion taken place at the basement-subbasement boundary, and is shown in Fig. III. 5. The time difference between the first arrival which is P-motion, and this phase, therefore gives the thickness of the formations overlying the subbasement. The following relations hold for these two phases.

$$T_1 = \frac{x}{V_6} + \eta(V_1,V_6)(h_1 + h_1') + \eta(V_2,V_6)(h_2 + h_2') + \eta(V_3,V_6)(h_3 + h_3') + \eta(V_4,V_6)(h_4 + h_4') + \eta(V_5, V_6)(h_5 + h_5')$$

$$T_2 = \frac{x}{V_6} + \eta(v_1,V_6)(h_1 + h_1') + \eta(v_2,V_6)(h_2 + h_2') + \eta(v_3,V_6)(h_3 + h_3') + \eta(V_4,V_6)(h_4 + h_4') + \eta(V_5,V_6)(h_5 + h_5')$$

---

* From well velocity survey

where $V_1, \ldots V_6$ are P-wave velocities in the layers and v_1, v_2, v_3 are S-wave velocities in the first three layers. Clearly the difference $(T_2 - T_1) = \Delta T$ gives the time taken by the wave to travel in the first three layers. The thickness of the sediments is known under the Suffield shot point and under the detectors. If H_1 is the combined thickness of the three layers under detectors and H_1' the same under shot point, the calculations yield as shown in table 6, a figure of average thickness 16.48 km for $(H_1 + H_1')$. Two or three of the detector positions for 500 ton profile lie very close to those for Bow City profile. The distance between Bow City and Suffield is 126.50 km. Some detector positions for both profiles are given below in table 5.

Table 5

Suffield Km	Bow City x Km	x + 126.50 Km
216.15	86.17	212.67
276.85	148.46	274.96
284.71	153.59	280.09
298.62	176.96	303.46

From the above table it can be easily seen that at least two of the detector positions are within 2-3 km. for both profiles; two of the positions are at least within 5 km. for both profiles. The information at these places is already known from Bow City profile.

From the Bow City profile, therefore, we take the following figures for the thickness of sediments and 6.16 layer.

Sediments	4.30 km
Basement	9.86 km
Thickness of sediments under Suffield	2.14 km
Total (average figure)	16.30 km

The corresponding figure as calculated from the converted phase for 500 ton profile is 16.48 km. This is evidence for extreme thinness (or absence) of the 6.16 layer under Suffield, as shown in Fig. III. 5. This was already pointed out in the interpretation under first arrival data.

The next converted phase occurs approximately 8 secs. after the first converted phase and approximately 10 secs. after the first arrival from the Moho. On the basis of intercept times this has been interpreted as the conversion taken place in the layers up to and including the subbasement. This therefore gives information about the subbasement.

The following relation holds for it.

$$T_7 = \frac{x}{V_6} + \eta(v_1,V_6)(h_1 + h_1') + \eta(v_2,V_6)(h_2 + h_2') + \eta(v_3,V_6)(h_3 + h_3')$$

$$+ \eta(v_4,V_6)(h_4 + h_4') + \eta(V_5,V_6)(h_5 + h_5')$$

where v_4 is the S-wave velocity in the subbasement.

Clearly $(T_7 - T_2) = \Delta T$ is given by

$$\Delta T = [\eta(v_4,V_6) - \eta(V_4,V_6)]\ (h_4 + h_4')$$

or

$$(h_4 + h_4') = \frac{\Delta T}{\eta(v_4,V_6) - \eta(V_4,V_6)} = \frac{\Delta T}{\Delta\eta}$$

Since all the quantities on right hand side are known one can calculate $(h_4 + h_4')$. These estimates are given in table 6. The average value for $(h_4 + h_4')$ is thus 51.62 km. But thickness of the subbasement under the Suffield shot point is 31.50 km. as calculated previously. This leaves a thickness of 20.12 km. for the subbasement under the detectors. It should be remembered here that the detectors are located quite far away from Suffield. Some detector positions are in the foothills while others are located deep in the mountains. This then says that the subbasement is getting thinner under the mountains. Further, this figure favorably compares with the thickness calculated for the same horizon in the Bow City profile in III. 6, the figure being 20.95 km.

The next converted phase occurs approximately 4.50 secs. after the second conversion and 14.50 secs. after the first arrivals from the Moho. This has been interpreted again on the basis of intercept times, as the conversion taken place in all layers above Moho. The equation for this is given below.

$$T_9 = \frac{x}{V_6} + \eta(v_1,V_6)(h_1 + h_1') + \eta(v_2,V_6)(h_2 + h_2') + \eta(v_3,V_6)(h_3 + h_3')$$
$$+ \eta(v_4,V_6)(h_4 + h_4') + \eta(v_5,V_6)(h_5 + h_5')$$

The difference $\Delta T = (T_9 - T_7)$ is thus

$$\Delta T = T_9 - T_7 = [\eta(v_5,V_6) - \eta(V_5,V_6)]\ (h_5 + h_5')$$

Table 6

	T_1	T_3			T_7			T_9	
x Km	PPPPPPP sec	SPPPPPS sec	T_3-T_1 sec	H_1+H_1' Km	SSPPPSS sec	T_7-T_3 sec	h_4+h_4' Km	SSSPSSS sec	T_9-T_7 sec
216.15	34.96	37.20	2.24	16.47	44.97	7.77	51.45	49.41	4.44
242.55	-	40.22	-	-	48.21	7.99	52.91	52.61	4.40
252.95	39.27	41.56	2.29	16.84	49.51	7.95	52.64	53.81	4.30
269.62	41.32	43.55	2.23	16.40	51.59	8.04	53.25	55.79	4.20
276.84	-	44.38	-	-	52.19	7.81	51.72	56.49	4.30
284.71	-	45.45	-	-	53.10	7.65	50.66	57.30	4.20
298.61	44.80	47.05	2.25	16.54	54.65	7.60	50.33	59.20	4.55
335.46	49.31	51.51	2.20	16.17	59.06	7.55	50.00	63.61	4.55

Average $h_5+h_5' = 25.23$ km. Average $H_1+H_1' = 16.48$ km. Average $h_4+h_4' = 51.62$ km.

or $$(h_5 + h_5') = \frac{\Delta T}{\Delta \eta}$$

where v_5, V_5 are S- and P-wave velocities in Intermediate Layer and h_5, h_5' are the thicknesses of this layer under detectors and shot point respectively.

This thus gives the thickness of the intermediate layer under the shot point and detectors combined. The average figure for this is 25.23 km. But the thickness of this layer under shot point as given under the interpretation of first arrival data is about 10 km. This leaves a thickness of about 15 km. under the detectors. This then says the intermediate layer is thicker under mountains.

The following picture for crustal layers thus arises from converted phases under the detectors.

Sediments	4.30 km
Basement	9.86 km
Subbasement	20.12 km
Intermediate Layer	15.23 km
Depth to Moho	49.71 km

III. 9 Converted Phases from Intermediate Layer

The first of these occurs round about 8 secs. after the first event from the intermediate layer. On the basis of intercept times this has been interpreted as a conversion taken place above the subbasement only under the shot point as shown in fig. III. 6. The

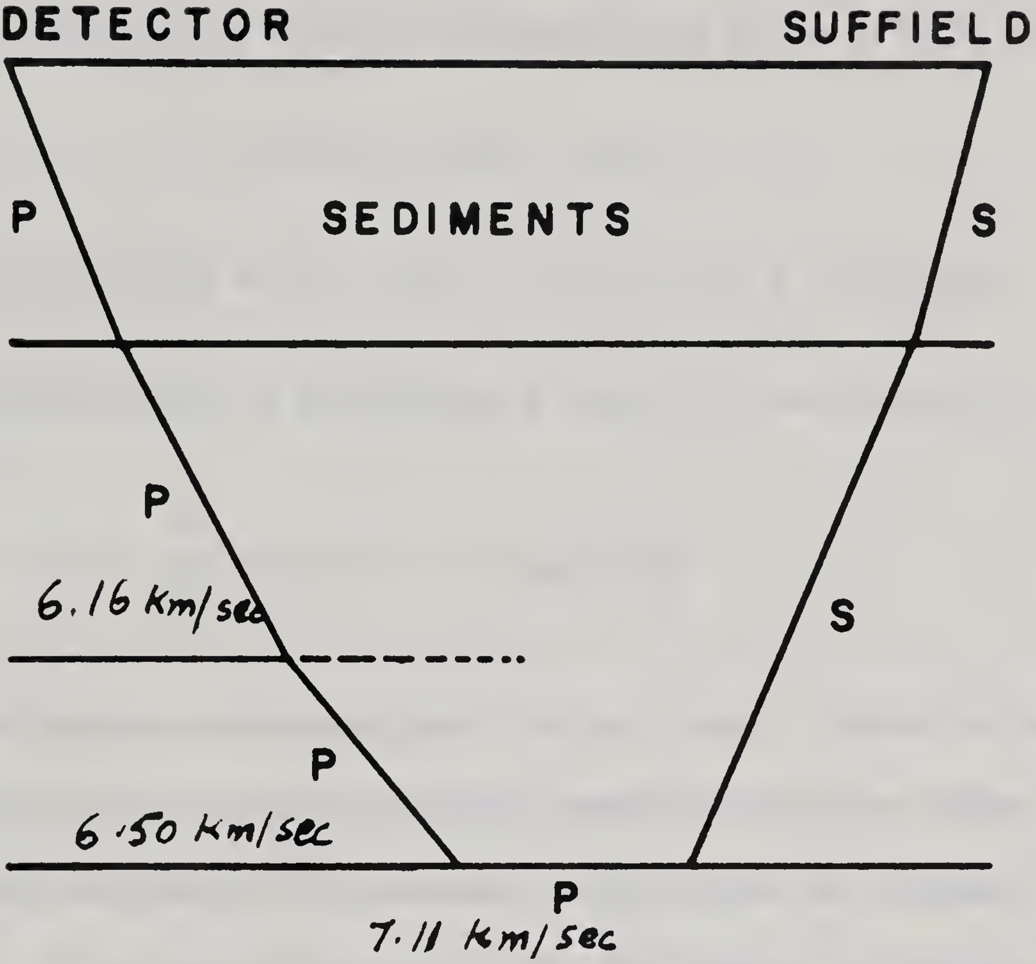
DETECTOR
SUFFIELD
P
SEDIMENTS
S
P
6.16 Km/sec
S
P
6.50 Km/sec
P
7.11 Km/sec

Fig. III. 6

rest of the path it travels as P-wave. The equation for this is given below as T_6. T_3 is the equation for the wave having the same path, except that it travels as P-wave throughout.

$$T_3 = \frac{x}{V_5} + \eta(V_1,V_5)(h_1 + h_1') + \eta(V_2,V_5)(h_2 + h_2') + \eta(V_3,V_5)(h_3 + h_3')$$

$$+ \eta(V_4,V_5)(h_4 + h_4')$$

$$T_6 = \frac{x}{V_5} + \eta(V_1,V_5)h + \eta(v_1,V_5)h_1' + \eta(v_2,V_5)h_2' + \eta(V_2,V_5)h_2$$

$$+ \eta(v_3,V_5)h_3' + \eta(V_3,V_5)h_3 + \eta(V_4,V_5)h_4 + \eta(v_4,V_5)h_4'$$

$$\Delta T = T_6 - T_3 = \sum_{i=1}^{4} [\eta(v_i,V_5) - \eta(V_i,V_5)]h_i'$$

h_i' is the thickness under shot point of $_i$th layer. Since the thicknesses of and velocities in sediments under Suffield are known one can calculate the thickness of subbasement which gives an average value of 30.26 km. This agrees favorably with the figure we obtained under the interpretation of first arrival which was 31.50 km.

Following this there is another arrival with the same spread velocity occurring about 4 secs. after the above arrival and about 12 secs. after the first event from the intermediate layer. It has been identified again on the basis of intercept times as a conversion taking place in the sediments and basement on one path and a conversion in the subbasement only, on the other part of the path. The equation for this is given by

$$T_8 = \frac{x}{V_5} + \eta(v_1,V_5)(h_1 + h_1') + \eta(v_2,V_5)(h_2 + h_2') + \eta(v_3,V_5)(h_3 + h_3')$$

$$+ \eta(v_4,V_5)h_4' + \eta(V_4,V_5)h_4$$

$$\Delta T = T_8 - T_6 = \sum_{i=1}^{3} [\eta(v_i,V_5) - \eta(V_i,V_5)]h_i$$

This thus gives a relationship between the time under and the thicknesses of, the sediments and basement under the detectors. Table 7 gives the thicknesses calculated for various layers on the basis of the converted phases from the intermediate layer. Knowing the thickness of sediments one can then calculate the thickness of basement. The thicknesses thus calculated at different distances are 8.49, 8.44, 8.49 with an average of 8.47 km. The average thickness for the same layer under Bow City profile was 9.86 km.

The crustal picture down to the intermediate layer from these calculations is as follows.

		Thickness km.	Velocity km/sec.
Suffield Shot Point			
Sediments	(Cretaceous	1.30	2.11
	(Mississippian	0.84	5.80
Subbasement		30.26	6.50
Detectors			
Sediments	(Cretaceous	2.14	3.00
	(Mississippian	1.16	5.80

Table 7

x_{Km}	T_1 PPPPP sec	T_2 SSPPP sec	T_3 SSPPS sec	T_3-T_2 sec	h_3 Km	T_2-T_1 sec	h'_4 sec
216.15	36.04	44.05	-	-	-	8.01	31.69
242.55	39.69	47.33	51.43	4.10	8.49	7.64	30.00
252.95	41.07	48.78	-	-	-	7.71	30.32
269.62	43.18	50.84	54.93	4.09	8.44	7.66	30.09
276.84	44.15	51.61	55.71	4.10	8.49	7.46	29.18
284.71	45.17	-	-	-	-	-	-
298.61	46.95	-	-	-	-	-	-
335.46	51.37	-	-	-	-	-	-

	Thickness km.	Velocity km/sec.
Basement	8.47	6.16
Subbasement	No informatnion	6.50

III. 10 S-Phases and Lg Phase

In addition to the various converted phases discussed above, S-phases from three horizons, the Subbasement, Intermediate Layer and Mohorovicić, were identified. Fig. III. 7 is a travel-time graph for these arrivals. Table 8 gives P and S velocities and Poisson's ratio for these layers.

Table 8

Horizon	Vp Km/sec	Vs Km/sec	Vp/Vs	σ
Subbasement	6.50	3.75	1.73	.249
Intermediate Layer	7.11	4.53	1.57	.159
Moho	8.37	4.73	1.76	.263

The following table gives the distances and time for the Lg Phase.

Table 9

Station	Distance (km.)	Time (secs.)	Velocity km/sec.
Kilo	218.15	61.12	3.57
Tango	243.55	67.65	3.60
Juliet	254.45	-	-
Hotel	270.62	72.21	3.75
Sierra	275.34	76.38	3.60
Lima	283.21	77.15	3.67
Papa	300.11	83.35	3.60

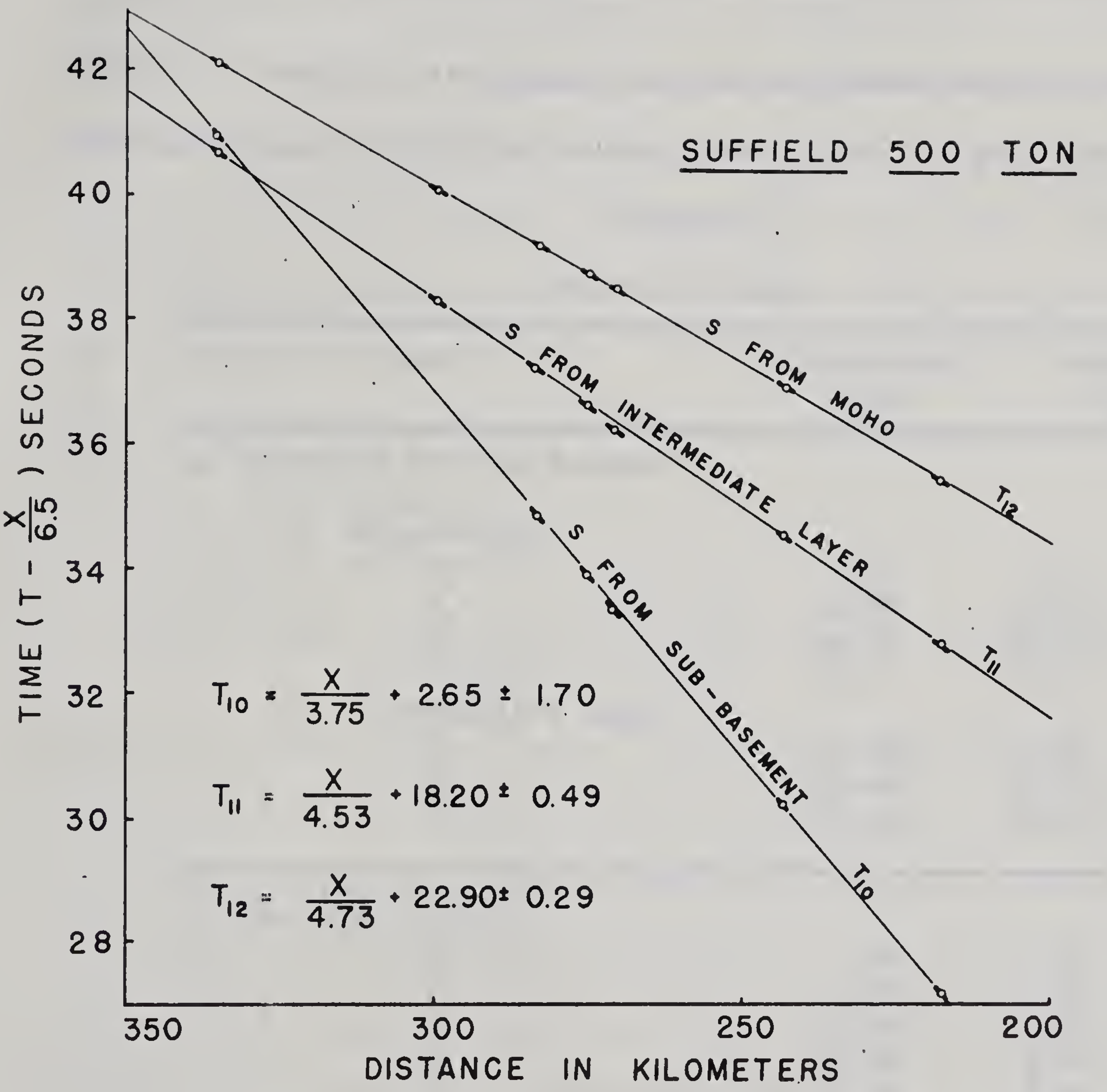
SUFFIELD 500 TON
S FROM MOHO
S FROM INTERMEDIATE LAYER
S FROM SUB-BASEMENT
T_{12}
T_{11}
T_{10}
$T_{10} = \frac{X}{3.75} + 2.65 \pm 1.70$
$T_{11} = \frac{X}{4.53} + 18.20 \pm 0.49$
$T_{12} = \frac{X}{4.73} + 22.90 \pm 0.29$
TIME $(T - \frac{X}{6.5})$ SECONDS
42
40
38
36
34
32
30
28
350
300
250
200
DISTANCE IN KILOMETERS

Fig. III. 7

This phase is particularly well displayed on the record at a distance of 218 km. where a clear onset and a dispersive wave train can be seen. The presence of this phase is another clear indication that S waves are generated by an explosive source at least in this particular case.

III. 11 In table 10 are enumerated the calculated and observed intercept times for all the events observed on both profiles.

Table 10

Intercept Times

Event	Calculated Time sec	Observed Time sec
a. Suffield 500 Ton Profile		
1. Mohorovicić		
T_1	9.24	9.25 ± .14
T_2	11.98	11.10 ± .33
T_7	19.31	18.75 ± 1.35
T_9	22.77	23.25 ± 0.55
2. Intermediate Layer		
T_3	5.63	5.60 ± .12
T_6	13.42	15.54 ± 1.10
T_8	18.23	18.92
b. Bow City Profile		
T_1	.87	.93 ± .05
T_2	1.97	1.95 ±
T_3	1.43	1.32 ± .07
T_5	2.42	2.46 ± .07
T_6	5.89	5.99 ± .05
T_7	8.54	8.64 ± .10
T_8	10.40	10.17 ± .08
T_9	13.95	14.50 ± .319

III. 12 Particle Motion Diagrams

In several cases where the event was of high quality with a good horizontal motion recorded, the particle motion diagram was drawn. These diagrams are shown in Figs. III. 8a and III. 8b. Polarisation of PS phase is not particularly clear from these diagrams, even though there is a large horizontal component of motion. The only bright feature about these diagrams for PS phases is that they indicate a predominantly horizontal motion with a phase difference between vertical and horizontal components. The following factors have to be borne in mind while collecting the records, in order to draw useful particle motion diagrams.

1. Orientation of horizontal geophones.
2. All the other factors mentioned under amplitude measurements below.

III. 13 The amplitudes of some of the events were measured. The ratios of amplitudes of the converted phases from the Mohorovicić to that of the P-event are plotted against the distance in Fig. 9a and the same for the basement and subbasement in Fig. III. 9b. A large scatter in the data is evident and it did not seem worthwhile to make detailed comparisons with theoretical values. If more data were available it might be possible to obtain some smoothed estimates of the amplitude ratios and hence obtain results which could be compared in a meaningful way to calculated values.

All the amplitude measurements are in arbitrary units and these

A 3a

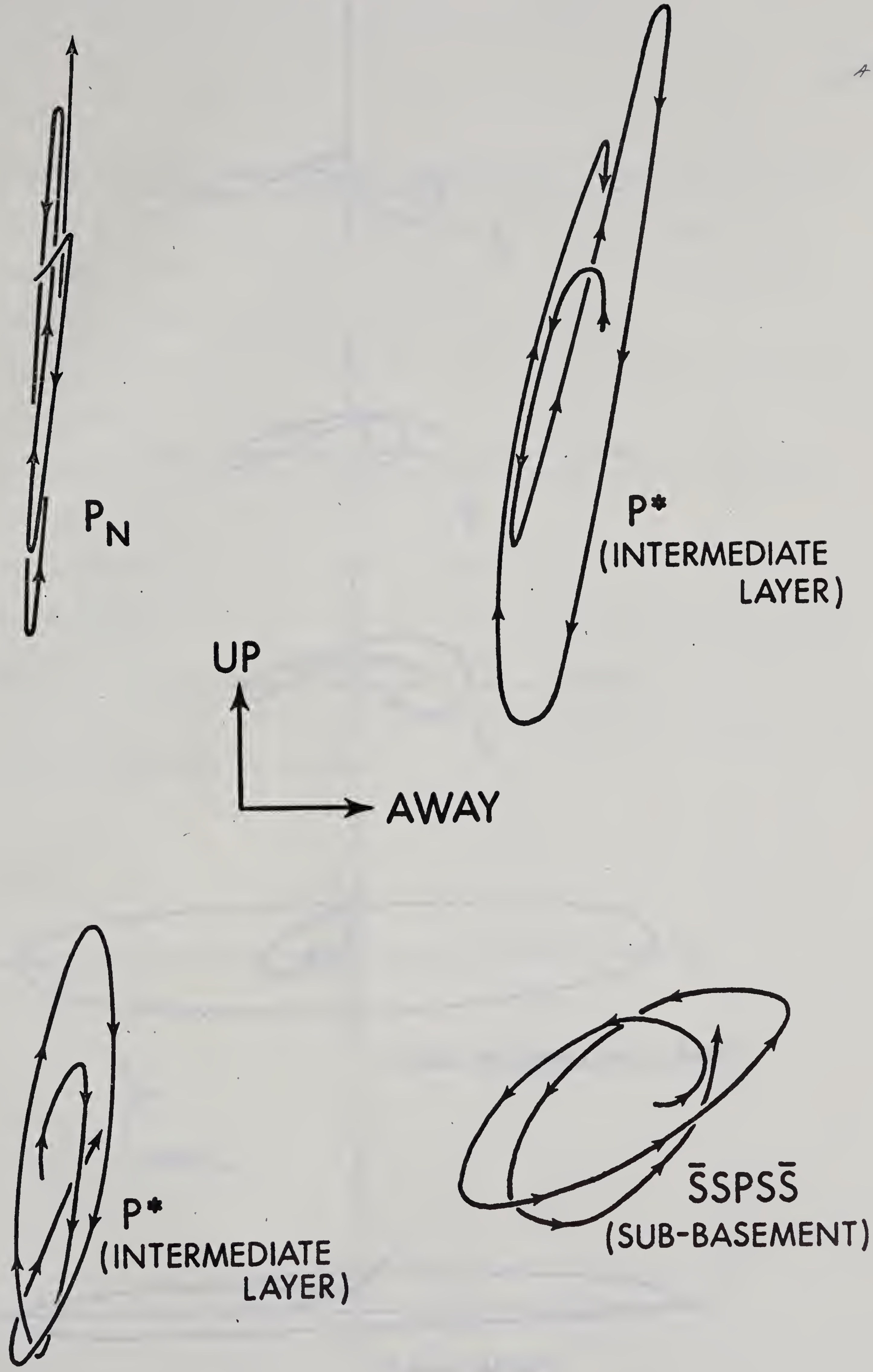

PARTICLE MOTION DIAGRAMS FOR SOME SELECTED EVENTS

Fig. III. 8a

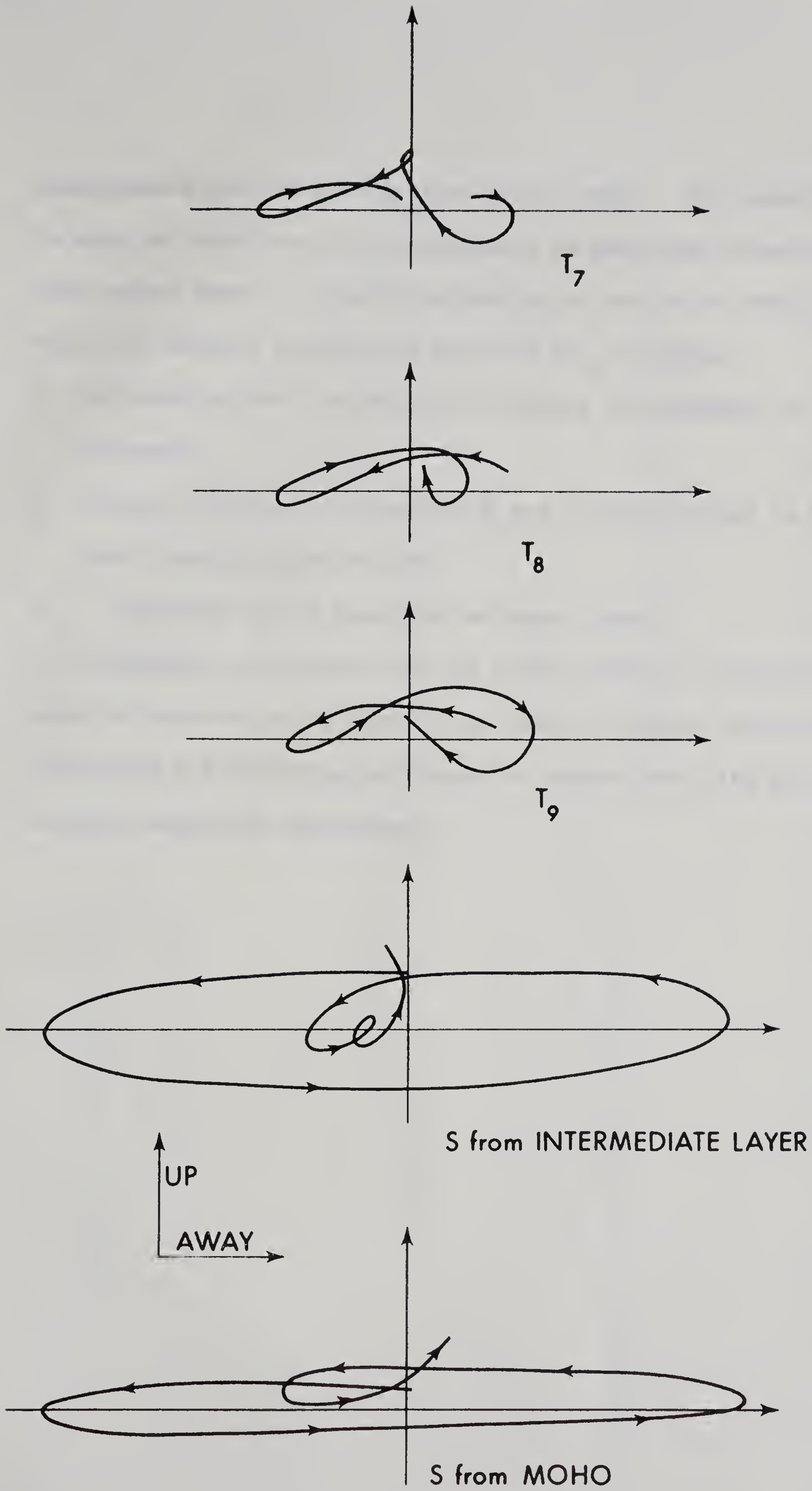

PARTICLE MOTION DIAGRAMS

Figure III 8b

measurements are not quantitative by any means. No comparison could be made as there were few measurements as mentioned already and no conclusions drawn. Certain features which are to be taken care of while the seismic surveys are done are the following.

1. Information about surface relief where the geophone is located is necessary.
2. Proper settings for attenuation and filter settings to be noted down clearly on the records.
3. Avoid as far as possible the power lines.
4. Preferably all records and all traces should be recorded on tape.

Once the records are on tape, it is easier to apply crosscorrelation techniques and filtering techniques to reduce the noise and get a more accurate amplitude measurement.

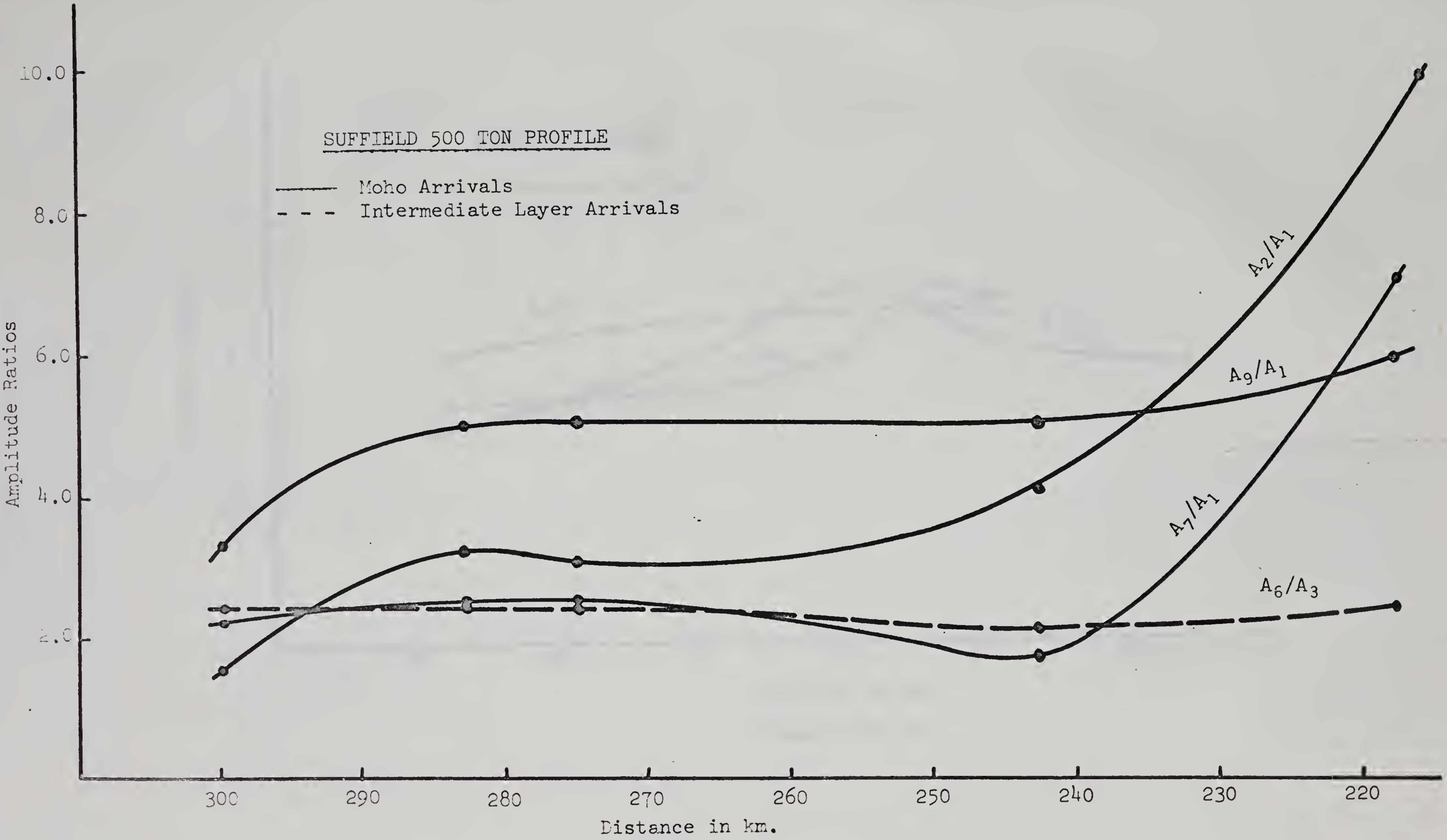

Figure III. 9a

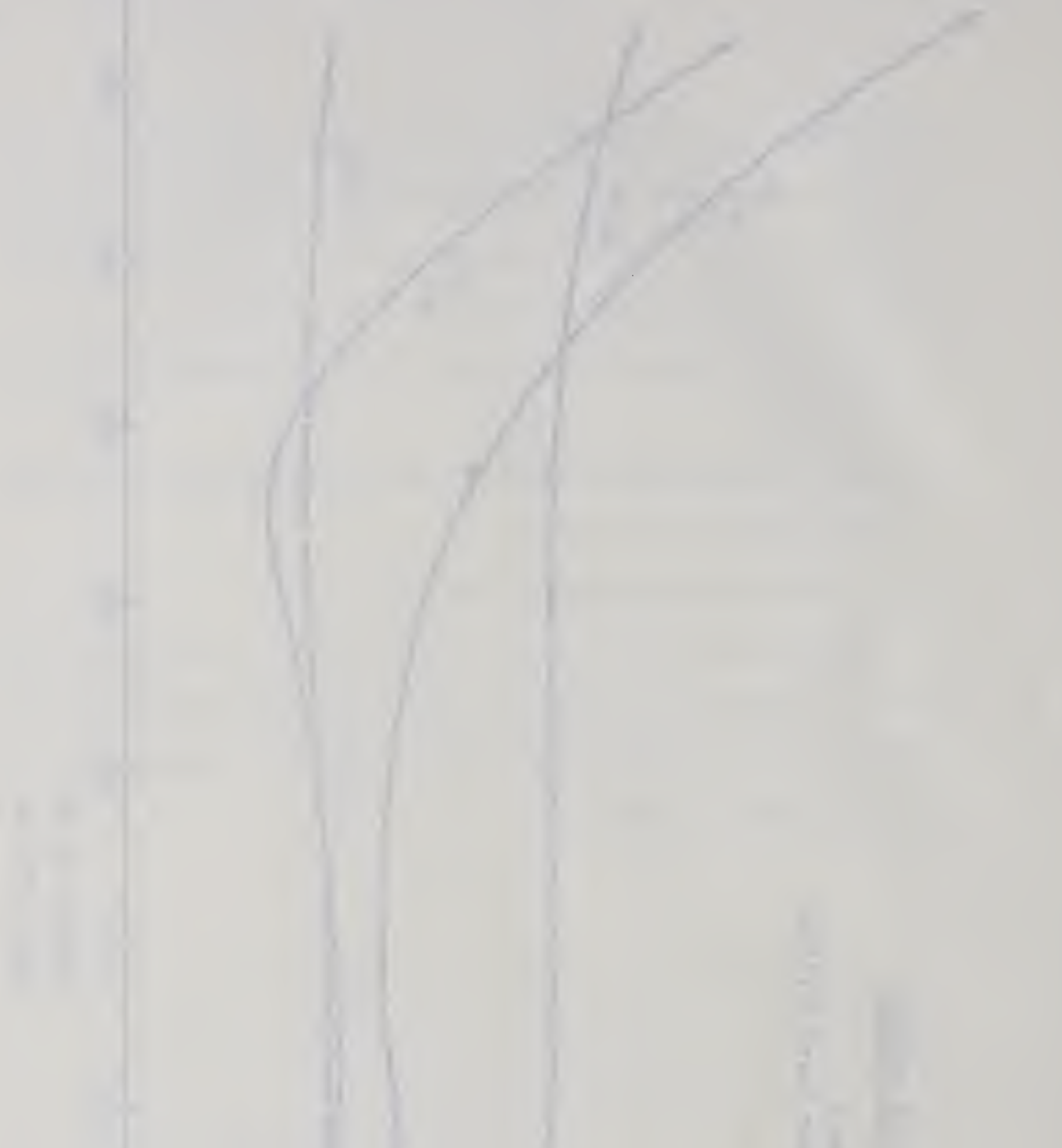

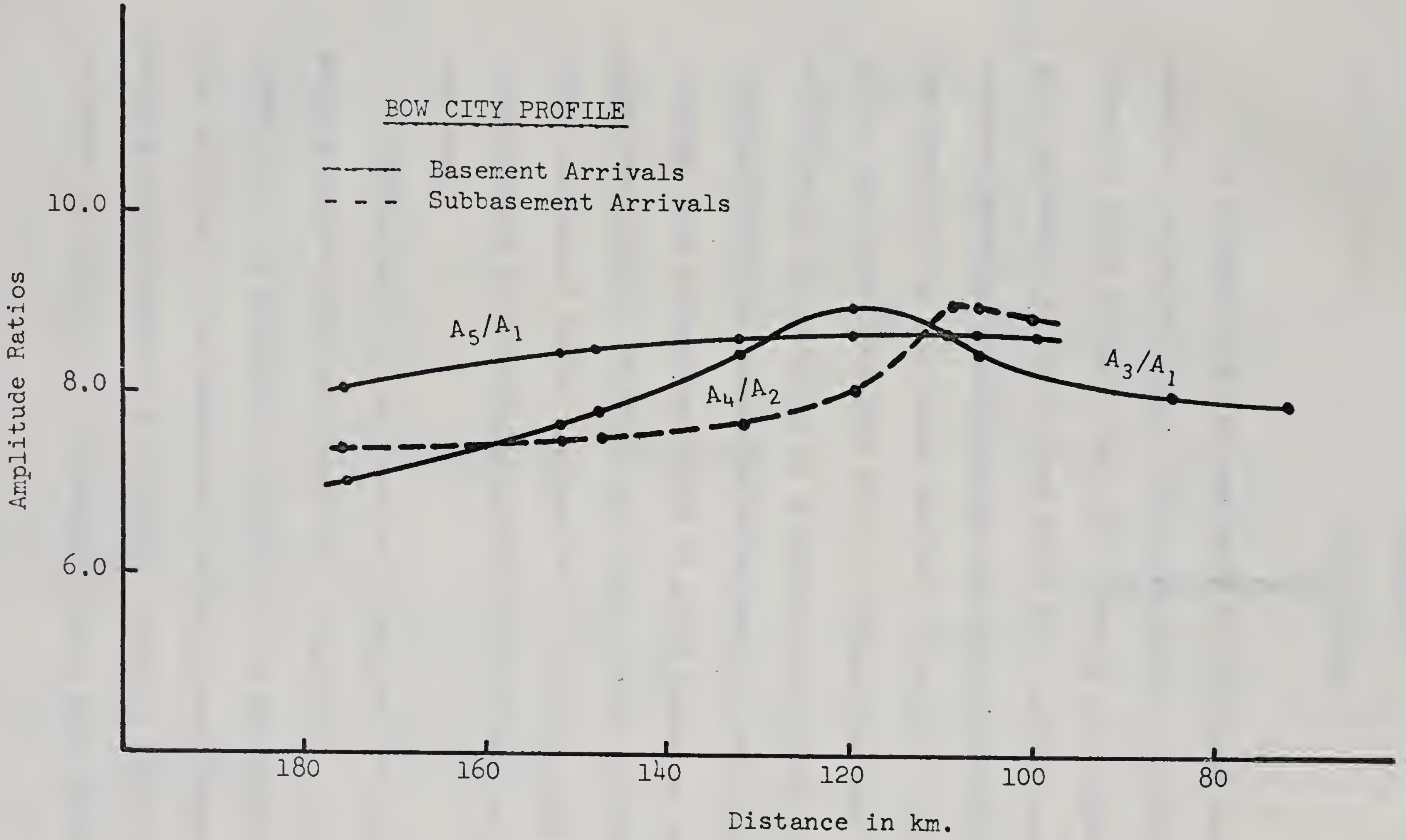

Figure III. 9b

CHAPTER IV

CONCLUSIONS

An attempt thus has been made to interpret various later events observed on two profiles. The calculations carried out based on the formulae given by Hall (loc. cit.) are in some cases in reasonably good agreement, while in some cases not, but the overall picture of crustal layering interpreted by this method is fairly convincing. The depth to the Moho under Suffield is about 44 km., under Bow City 48 km. and under the mountains 49 km. Remembering that Bow City is west of Suffield, this picture of a deeper Moho towards the west is in agreement with the conception of thickening crust under the Rockies, although this thickening is not as great enough to suggest a root under the Rockies. Further this figure of 49 km. must have rather large confidence limits assigned to it and hence the value is considered to be in reasonable agreement with other estimates in the same area.

Taking layer by layer we see first that the sediments are getting thicker near the foothills. (Figs. IV. 1, IV. 2) This agrees with the geological evidence of the occurrence of Mississippian outcrops in the mountains. Secondly the basement itself is getting thinner under the mountains. Thirdly the subbasement does the same and lastly the intermediate layer gets thicker under mountains.

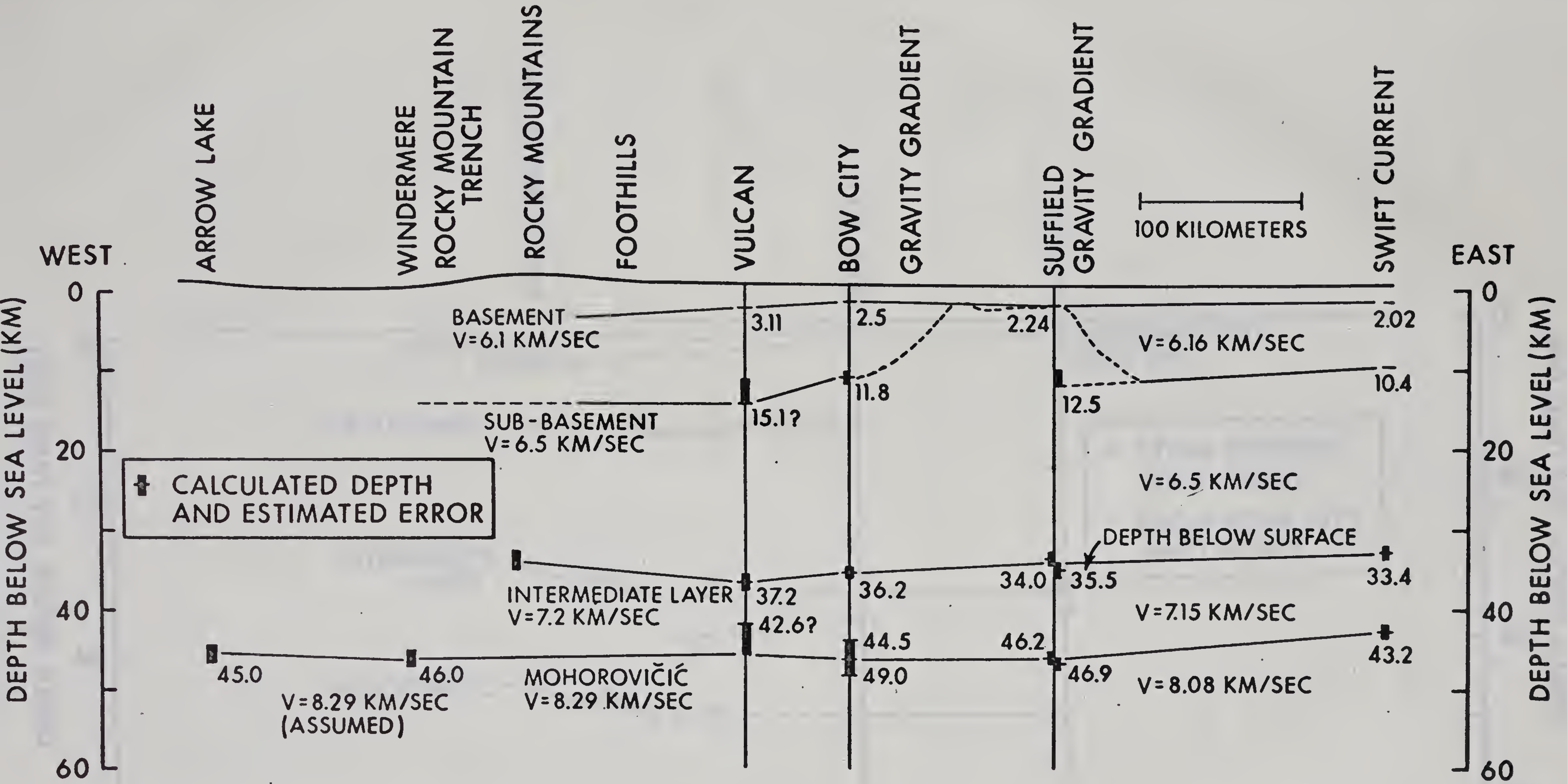

CRUSTAL THICKNESS IN WESTERN CANADA

Fig. IV 1

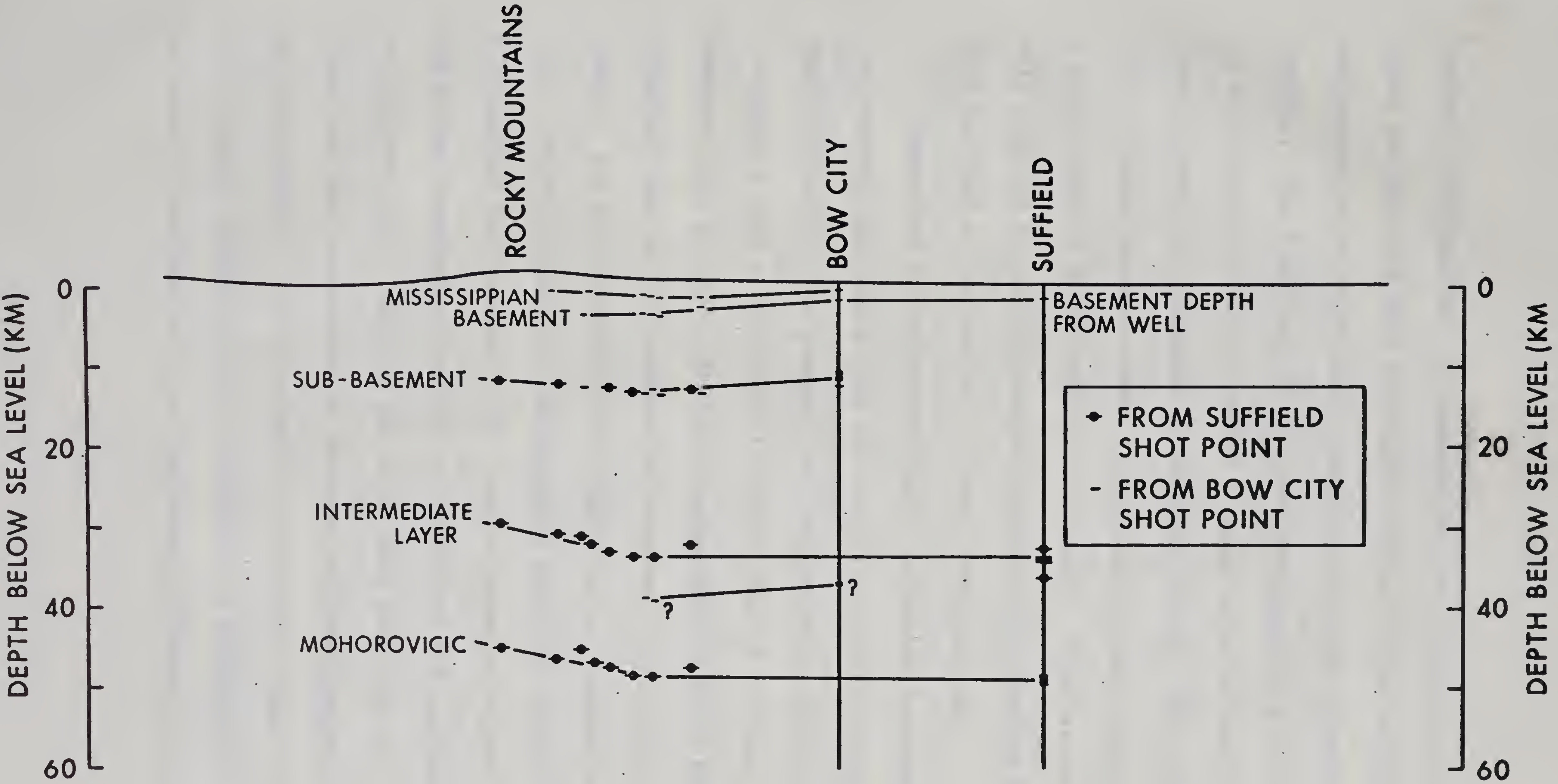

DEPTH ESTIMATES FROM CONVERTED PHASES

Fig. IV. 2

Certain discrepancies, for example in the thickness of the subbasement under the Bow City shot point, did occur in these calculations. This is because of the very small quantities involved in many of the calculations. The functions $\eta(U_i,U_j)$ are very small and the difference $\Delta\eta$ is still smaller with the result a change even in the third decimal place affects the thickness by at least 3-4 km. This ultra sensitiveness of these functions makes it necessary to know the true velocity in a given layer to a high degree of accuracy. This was not achieved in this case due to lack of reverse control on the various horizons. This has been a big handicap in these investigations.

Comparison of the theoretically calculated intercept times with the observed ones shows that for the first arrivals these two agree reasonably well. For example the first arrivals on the Suffield 500 ton profile have a calculated intercept time of 9.24 sec. against the observed 9.25 sec. For Bow City the basement arrivals have a calculated intercept time of 0.87 against the observed 0.88 (taking the lower limit.) For the subbasement the figure is 1.97 against an observed 1.95. The same figure for intermediate layer for Suffield 500 ton is 5.63 against the observed 5.60. Most of these calculated times thus are either reasonably close to, or within the 90% confidence limits of, the observed ones. Mention has to be made here that all the intercept times have been calculated on the basis of first arrival data. Hence any discrepancy in the calculation of intercept times for later arrivals can be easily understood as a consequence of applying the results of one event to another which are completely different in character.

BIBLIOGRAPHY

Andreev, S.S., A study of the plutonic structure of the earth's crust using PS exchange waves recorded during earthquakes, Bull. Acad. Sci. USSR, Geophys. Ser. (English Translation), 1, 22-31, 1957.

Branson, E.B. and W.A. Tarr, Introduction to Geology, McGraw Hill, 1955.

Cook, K.L., S.T. Algermissen, and John K. Costain. The Status of PS Converted Waves in Crustal Studies, Journal of Geophysical Research, Vol. 67, No. 12, 4769-4778, 1962.

Cumming, G.L., G.D. Garland and K. Vozoff. Seismological Measurements in Southern Alberta, Final Report, Contract AF19(604)-8470, Project Vela-Uniform, 1962.

Cumming, G.L. and E.R. Kanasewich, Crustal Structure in Western Canada, Final Report, Contract No. AF19(628)-2835, Project Vela-Uniform, 1966.

Cumming, G.L. and G.T. Maureau, Crustal Structure in Western Canada, Scientific Report #1, Contract AF19(628)-2835, Project Vela-Uniform, 1964.

Ewing, W.M., W.S. Jardetzky and F. Press, Elastic Waves in Layered Media, McGraw-Hill Book Company, Inc., 1957

Gutenberg, B., Energy ratio of reflected and refracted seismic waves, Bull. Seismol. Soc. Am., 34, 85-102, 1944.

Hall, D.H., Converted Waves in Refraction Surveys over Markers with Variable Depth, Geophysics, Vol. XXIX, No. 5, 733-744, 1964.

Hall, D.H., The Converted-Wave Method of Seismic Refraction Interpretation for Interfaces with Severe Dip and Curvature, Canadian Journal of Earth Sciences, Vol. 3, 111-125, 1966.

Hall, D.H. and W.C. Brisbin, Crustal Structure from Converted Head Waves in Central Western Canada, Geophysics, Vol. XXX, No. 6, 1053-1067, 1965.

Heelan, P.A., On the theory of head waves, Geophysics, Vol. XVIII, 871-893, 1953.

Jeffreys, H., The reflection and refraction of elastic waves, Monthly Notices Roy. Astron. Soc., Geophys. Suppl., I, 321-334, 1926.

Knott, C.G., Reflexion and refraction of elastic waves, with seismological application, Phil. Mag. (5) 48, 64-97, 1899.

Macelwane, J.B. and F.W. Sohon. Introduction to Theoretical Seismology, Part I, St. Louis University, 1932.

Maureau, G.T., Crustal Structure in Western Canada, M.Sc. Thesis, University of Alberta, 1964.

Muskat, M., Theory of Refraction Shooting, Physics, 4, 14-28, 1933

Muskat, M., and M.W. Meres, Reflection and transmission coefficients for plane waves in elastic media, Geophysics, 5, 115-148, 1940.

Nafe, J.E., Reflection and transmission coefficients at a solid-solid interface of high velocity contrast, Bull. Seismol. Soc. Am., 47, 205-219, 1957.

Pakiser, L.C., and D.P. Hill, Crustal Structure in Nevada and Southern Idaho from Nuclear Explosions, Journal of Geophysical Research, Vol. 68, No. 20, 5757-5766, 1963.

Richards, T.C., Motion of the ground on arrivals of reflected longitudinal and transverse waves at wide-angle reflection distances, Geophysics, 26, 277-297, 1961.

Scwhind, J.J., J.W. Berg, Jr., and K.L. Cook, PS Converted Waves from Large Explosions, Journal of Geophysical Research, Vol. 65, No. 11 3817-3824, 1960.

Steinhart, J.S. and R.P. Meyer, Explosion Studies of Continental Structure, C.I.W. Publication, No. 622, 1961.

Weaver, D., Crustal Thickness in Southern Alberta, M.Sc. Thesis, University of Alberta, 1962.